The mechanical and chemical stability of the interfaces in bioactive materials: The substrate-bioactive surface layer and hydroxyapatite-bioactive surface layer interfaces

Materials Science & Engineering C 116 (2020) 111238

Contents lists available at ScienceDirect

Materials Science & Engineering C

journal homepage: www.elsevier.com/locate/msec

The mechanical and chemical stability of the interfaces in bioactive materials: The substrate-bioactive surface layer and hydroxyapatite-bioactive surface layer interfaces

S. Ferraris[a], S. Yamaguchi[b], N. Barbani[c], C. Cristallini[d], G. Gautier di Confiengo[e], J. Barberi[a], M. Cazzola[a], M. Miola[a], E. Vernè[a], S. Spriano[a,*]

[a] Politecnico di Torino, Corso Duca degli Abruzzi 24, 10129 Torino, Italy
[b] Chubu University, 1200 Matsumoto cho –, Kasugai, Japan
[c] University of Pisa, DICI – Largo Lucio Lazzarino 1, 56126 Pisa, Italy
[d] CNR, IPCF - Largo Lucio Lazzarino 1, 56126 Pisa, Italy
[e] CNR, IMAMOTER – Strada delle Cacce 73, 10135 Torino, Italy

ARTICLE INFO

Keywords:
Bioactive materials
Interfaces
Surfaces
Stability
Scratch resistance
Hydroxyapatite

ABSTRACT

Bioactive materials should maintain their properties during implantation and for long time in contact with physiological fluids and tissues. In the present research, five different bioactive materials (a bioactive glass and four different chemically treated bioactive titanium surfaces) have been studied and compared in terms of mechanical stability of the surface bioactive layer-substrate interface, their long term bioactivity, the type of hydroxyapatite matured and the stability of the hydroxyapatite-surface bioactive layer interface. Numerous physical and chemical analyses (such as Raman spectroscopy, macro and micro scratch tests, soaking in SBF, Field Emission Scanning Electron Microscopy equipped with Energy Dispersive Spectroscopy (SEM-EDS), zeta potential measurements and Fourier Transformed Infra-Red spectroscopy (FTIR) with chemical imaging) were used. Scratch measurements evidenced differences among the metallic surfaces concerning the mechanical stability of the surface bioactive layer-substrate interface. All the surfaces, despite of different kinetics of bioactivity, are covered by a bone like carbonate-hydroxyapatite with B-type substitution after 28 days of soaking in SBF. However, the stability of the apatite layer is not the same for all the materials: dissolution occurs at pH around 4 (close to inflammation condition) in a more pronounced way for the surfaces with faster bioactivity together with detachment of the surface bioactive layer. A protocol of characterization is here suggested to predict the implant-bone interface stability.

1. Introduction

Implantable biomaterials are intended for long term contact with biological tissues and, in many cases, for integration with these tissues. Upon implantation, the material surface comes in contact with the physiological fluids and absorption of water, ions and proteins occurs followed by cell adhesion, which is influenced by the previously formed protein layer [1].

Numerous innovative biomaterials, surface treatments and coatings have been developed in order to tailor the biological response of implanted materials [2–5]. All these engineered surfaces should maintain their peculiar features after implantation and in contact with the biological fluids and tissues. This means that the interface between the surface bioactive layer/coating and the bulk substrate should be stable in working condition, otherwise the surface effectively exposed to the biological environment will not be the designed one. In particular, they should sustain implantation load and friction [6] without alteration and maintaining their properties even after prolonged contact with physiological fluids [7,8], in order to promote bone integration and avoid the development of excessive inflammatory processes.

In the case of bioactive materials, the evaluation of chemical and mechanical stability is even more complex because these surfaces, upon contact with the physiological fluids, react and progressively form an hydroxyapatite layer which can chemically bond to the bone. This step is fundamental for a rapid and stable bone integration, but introduces a second interface (hydroxyapatite-bioactive surface layer) which should be enough stable to guarantee physiological and durable bone integration without excessive inflammation.

* Corresponding author.
E-mail address: silvia.spriano@polito.it (S. Spriano).

https://doi.org/10.1016/j.msec.2020.111238
Received 10 April 2020; Received in revised form 5 June 2020; Accepted 23 June 2020
Available online 25 June 2020

The development of innovative bioactive materials for bone integration by means of surface modification or coatings is widely investigated in the scientific literature. The adhesion of coatings and the mechanical resistance of the bioactive surface layers is usually investigated by means of scratch, micro or nano indentation, tensile, bending and pull out tests [9–18] and often correlated with the ability of surface pretreatments to improve it. Moreover, the mechanical stability of the surface is usually investigated by means of wear tests [9,14], while the chemical stability is mainly studied as corrosion resistance in contact with simulated physiological fluids [7–9,14,19]. Behavior of the surface in a biological environment is mainly studied in terms of biomolecule release at the interface, protein absorption ability, cell adhesion and proliferation, in in vitro tests, as well as bone deposition and strength of bone bonding (removal force) after in vivo tests [10,12–14,19–24].

On the other hand, the mechanical and chemical stability of bioactive materials after soaking in Simulated Body Fluid (SBF), as a simulation of material surface stability after prolonged contact with physiological fluids, has never been reported. Moreover, the possible correlation between surface reactivity (e.g. fast/slow bioactivity) and the stability of the bioactive layer-substrate interface and of the hydroxyapatite-bioactive surface layer has not been yet deeply investigated. The above reported gap of knowledge are the main focus of the present research.

In the present research work, in fact, a bioactive glass and four different chemically treated bioactive titanium surfaces have been studied in order to investigate and compare the mechanical stability of the surface bioactive layer (that is the silica gel in the case of a bioactive glass and the modified oxide layer in the case of Ti based materials)-substrate interface, their long term bioactivity (hydroxyapatite precipitation ability in Simulated Body Fluid – SBF up to 28 days), the type of hydroxyapatite matured on the different surfaces and also, for the first time, the stability of the hydroxyapatite- surface bioactive layer interface.

The materials have been selected, among the authors developed ones, as representative of different classes of materials (metals and bioactive glasses) and mechanisms/kinetics of bioactivity, as previously reported by the authors [25]. This kind of study has never been reported in the scientific literature nor for these materials nor for others, so it has a double aim: to give a comparison of the behavior of the here selected materials (from a new standpoint) and to give a new method for comparison of different bioactive materials.

Raman spectroscopy, macro and micro scratch tests, soaking in SBF, Field Emission Scanning Electron Microscopy equipped with Energy Dispersive Spectroscopy (SEM-EDS), zeta potential measurements and Fourier Transformed Infra-Red spectroscopy (FTIR) with chemical imaging were used as complementary techniques for an in depth investigation of the above described mechanisms.

2. Materials and methods

2.1. Samples preparation

A bioactive glass (BG, 48% SiO_2, 18% Na_2O, 30% CaO, 3% P_2O_5, 0.43% B_2O_3, 0.57% Al_2O_3%mol) was synthesized by the melt and quenching technique [25,26]. Glass slices (2 mm thick, 10 mm diameter) were obtained by automatic cutting (ATA, Brillant) from the poured and annealed glass cylinder and subsequently polished by SiC abrasive papers up to 1000 grit. The BG was not surface treated in any way.

10 × 10 × 1 mm pure Ti (ISO5832-2, Nilaco Co., Tokyo, Japan) and Ti-6Al-4 V alloy (ASTM B348, Gr5Titanium Consulting and Trading, Buccinasco, Italy) plates were abraded with #400 diamond plates, washed with acetone, 2-propanol and ultrapure water (30 min, ultrasonic bath) and, then dried at 40 °C. These materials were used as substrates for the following treatments aimed at the obtainment of bioactive metallic surfaces [25,27–29].

Ti(A-HC-H) samples were soaked in 5 M NaOH alkali solution at 60 °C for 24 h, and subsequently in 50 mM HCl at 40 °C for 24 h, then heat treated at 600 °C for 1 h [25,28].

Ti64(A-H) samples were soaked in the NaOH solution at 95 °C for 24 h and then the heat treated [25,29].

Ti64(A-Ca-H-W) samples were soaked in the NaOH solution at 95 °C for 24 h, then in 100 mM $CaCl_2$ solution at 40 °C for 24 h followed by the heat treatment and finally by hot water treatment at 80 °C for 24 h [25,29].

Ti64(HF-H_2O_2) samples were acid etched in diluted hydrofluoric acid and then underwent a controlled oxidation in hydrogen peroxide [25,27].

2.2. Raman spectroscopy

Since the thickness of the modified layers is limited (400 nm – 1.6 μm for metallic surfaces and no modified layer in the case of the bioactive glass), as previously reported by the authors [25,27–29] its crystalline structure was investigated by means of Fourier transform confocal laser Raman spectrometer (FT-Raman: LabRAMHR800, Horiba Jobin Yvon, Longjumeau, France) with the measurement conditions of 514.5 nm of Ar laser and 16 mW of power excitation. One sample per type was analyzed by Raman spectroscopy.

2.3. Scratch resistance

Scratch adhesion test is a quick method to evaluate coating adhesion, but sometime is difficult to express adhesion in a quantitative way because the critical load is influenced by many factors such as substrate, film thickness, hardness, interface bonding. Moreover, critical load depends on the several parameters related to the test conditions such as indenter radius R, scratch speed and loading rate.

In this work, the different adhesion of the surface bioactive layers was measured and compared with a macro and micro scratch test. For both tests at least 3 tracks were performed for each sample type.

The micro and macro test were performed in order to have a complete adhesion characterization. Indeed, with an increasing indenter tip scale, can be reproduce both submicroscopic that macroscopic contacts.

2.3.1. Macro-scratch resistance

Macro-scratch tests were performed in Revetest mode (CSM™ Revetest machine) in order to determine the scratch resistance of the surface oxide layers and of the glass surface, as well as the adhesion of surface oxide layers to the metallic substrates. A progressive load (1–50 N) was applied on the surface through a Rockwell C diamond indenter with 200 μm diameter (Fig. 3d). The total scratch length track was 4.9 mm and the indenter speed 10 mm/min, as suggested in [30]. 3 tracks were performed on each sample. A reduced track length (3.75 mm) and final applied load (38.51 N) were considered for the glass sample (maintaining the same indenter speed (10 mm/min) in order to avoid fragile rupture of thin glass slice.

The tracks were observed by means of an optical microscope and the the critical loads were evaluated according to “Scratch Test Atlas of Failure Modes” cited in the Draft of European Standard prEN1071–3.

Tridimensional profile were done on Ti64(A-H), Ti(A-HC-H), Ti64(A-Ca-H-W) and Ti64(HF-H_2O_2), in order to verify scratch depth along the track and to evaluate the deformation outside scratch track. Tridimensional analysis was carried out with a Taylor Hobson type Form Talysurf 120 L measuring machine.

2.3.2. Micro-scratch resistance

The micro scratch resistance of the surface layer to the metal substrate was examined by a thin-film scratch tester (CSR-2000, Rhesca Co., Ltd., Tokyo, Japan) according to JIS R-3255. A stylus diamond with diameter of 5 μm (Fig. 4c) and spring constant of 200 g/mm was

pressed into the treated metal surface under the conditions of scratch speed of 10 μm/s, loading rates of 100 mN/min, and amplitude of 100 μm. Maximum load was set as 100mN, but measurement was manually stopped immediately when the surface layer was removed to protect the stylus. Five measurements were performed on each sample, and their averaged values were used for analysis.

2.4. In vitro bioactivity evaluation

In vitro bioactivity, as the surface ability to induce hydroxyapatite precipitation in Simulated Body Fluid (SBF), was investigated by samples soaking in 25 ml of SBF following the protocol of Kyoto University as suggested by the ISO standard [31,32] at 37 °C for different experimental times: 1 day, 7 days and 28 days. In this last case, SBF solution was refreshed weekly. Experimental times have been selected following this rationale: shorter times (less than 1 day) were previously investigated by the authors [25] and they are not useful in the context of this paper, because the hydroxyapatite layer is too thin to investigate the stability of the interface. 1, 3 and 7 days monitor the evolution of the hydroxyapatite crystals, while 28 days is effective to better investigate behavior of slow bioactive materials (e.g. Ti64(HF-H2O2)): the stability of the interface after the formation of a very thick apatite layer, that is the focus of this paper, can be measured. In fact, 28 days or 1 month is the experimental time often used after in vivo tests to check for osseointegration. 4 samples per type were tested for in vitro bioactivity.

2.5. Zeta potential titration

The zeta potential measurements were performed on as-prepared and SBF soaked (at different set points, 1, 7 and 28 days) samples by means of an electrokinetic analyzer (SurPASS, Anton Paar) in order to investigate the surface modifications occurred during soaking in SBF and to estimate the chemical stability of the surface oxide layers and/or precipitated hydroxyapatite. The tests were performed using KCl (0.001 M) as a electrolyte. For each type of sample, the measurements were conducted on the same set of specimens, considering at first a washing up of the instrument, a basic titration (NaOH 0.05 M addition through the instrument automatic titration unit) followed by instrument and sample washing with ultrapure water (2 cycles with 500 ml water) and acid titration (HCl 0.05 M addition to freshly prepared KCl, through the instrument automatic titration unit). This type of measurement foresees the mounting of a couple of specimens in the instrument cell, with the formation of a gap between them (Fig. 1). The electrolyte flows through the gap and causes the motion of the layers of charges developed at the interface and the consequent development of a potential difference at the edges of the cell (streaming potential), which is measured by the instrument and used for the calculation of the zeta potential [33,34]. During the measurement setup the gap is set to a value close to 100 μm and the electrolyte flow to at about 100 ml/min, as suggested in [33]. The Isoelectric Point (IEP) is identified as the intersection of the titration curve with the horizontal axis (zeta potential equal to 0 mV). The evaluation of the gap and its eventual change (it will be called “Delta of the gap” and it is value of the measured gap at each point subtracted of the value of the initial gap) during the test can give complementary information on the eventual detachment of surface layers occurring during the measurements. It was considered as a significant change if the delta of the gap is higher than 5 μm.

2.6. Field emission scanning electron microscopy observations

Field Emission Scanning Electron Microscopy equipped with Energy Dispersive Spectroscopy (FESEM-EDS, Merlin Gemini, Zeiss and Hitachi Co., Tokyo, Japan & Horiba Ltd., Kyoto, Japan) was used for morphological and chemical analyses of the sample surface before and after soaking in SBF (1, 7 and 28 days) and also after zeta potential measurements before and after soaking in SBF. FESEM analyses allow the observation of surface morphology at the micro-nano scale, of hydroxyapatite precipitation after SBF soaking as well as of eventual surface alterations induced by zeta potential measurements. EDS analyses performed during observation allows to confirm the surface layer compositions and hydroxyapatite identification.

Cross section of the samples after soaked in SBF were exposed by bending the samples [35] and subjected to carbon coating, which was subjected to SEM observation to estimate thickness of hydroxyapatite layer. EDS analysis was used to confirm hydroxyapatite identification, again.

2.7. FTIR chemical imaging

Spectral images were carried out by means of a Perkin Elmer Spectrum Spotlight 300 FT-IR Imaging System, in the μATR mode. An area of 1 mm × 1 mm was analyzed and an IR image was produced using a liquid nitrogen cooled, 16-pixel mercury cadmium telluride (MCT-A) line detector. All spectra were recorded in the mid infrared region (4000–750 cm^{-1}) at 16 scans per pixel; the spectral resolution was 4 cm^{-1}; the spatial resolution was 100 × 100 μm. The acquired chemical map was used to obtain the average spectrum, the most representative spectrum of the chemical map. The spectral maps were

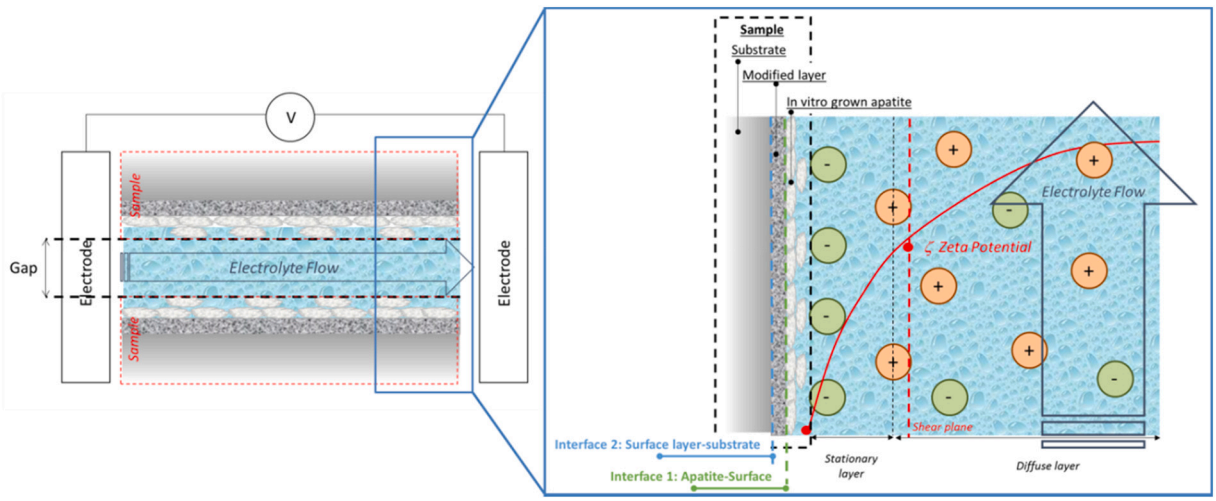

Fig. 1. Schematization of zeta potential electrokinetic measurements, with details of the investigated interfaces.

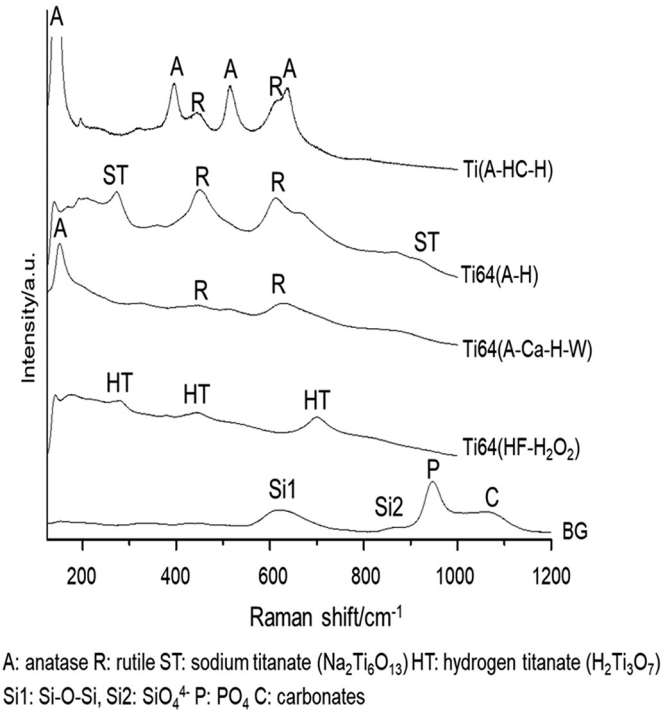

Fig. 2. Raman spectra of the as prepared samples.

elaborated using spotlight software to obtain correlation maps and the band absorbance ratio. Band ratio analysis was used to evaluate the degree of carbonation by using an area-based method [25].

3. Results

3.1. Crystalline structure of the surfaces: Raman spectroscopy

Investigation of the crystalline structure of the samples is relevant in the evaluation of their bioactivity, chemical and mechanical stability. Raman spectroscopy was selected for investigating the surface crystalline structure of the samples because it is most suitable than X ray diffraction (XRD) to investigate a wide range of materials with surface bioactive layers of different thickness, even as thin as few hundreds of nanometers (as in the case of Ti64(HF-H_2O_2)) where XRD was not suitable (sampling depth in the micron range, too high influence of the substrate in the spectrum for thin layers). The Raman spectra of as prepared (before SBF soaking) samples are reported and compared in Fig. 2.

Anatase and rutile can be detected on Ti(A-HC-H) (mainly anatase) and Ti64(A-Ca-H-W), while sodium titanate and rutile on Ti64(A-H). Calcium titanate ($CaTi_2O_4$, $CaTi_2O_5$ and $CaTi_4O_9$) on Ti64(A-Ca-H-W) reported in a XRD measurement [29] cannot be identified in this Raman analysis. The main phase on Ti64(HF-H_2O_2) can be identified as $H_2Ti_3O_7$.

The structure of the bioactive glass (BG) silicate is amorphous and through the Raman Spectroscopy phosphate and carbonate groups can be observed. In particular, Si-O-Si groups have a signal at about 635 cm^{-1}, monomers SiO_4^{4-} at about 860 cm^{-1} while symmetrical stretching of PO_4^{3-} can be observed at about 950 cm^{-1} and carbonate groups at 1070 cm^{-1} [36].

3.2. The substrate–bioactive surface layer interface: the macro scratch test

Considering that during the surgical implantation procedure and implant life, scratches due to a wide range of applied load can occur, scratch tests were performed exploring a wide range of conditions.

Macro-scratch tracks of the samples with comparison of the critical loads are shown in Fig. 3.

Low magnification observation of the whole scratch tracks (Fig. 3a) allows a comprehensive comparison between the materials. The appearance of grey-shiny spots or areas can be associated with the exposure of the metallic substrate for titanium samples. The load at which this first damage occurs can be defined as the first critical load (LC1) and denoted as First Damage of the surface layer (Fig. 3 b and c). It can be noted that this phenomenon occurs at the beginning of the track for Ti64(A-H) and Ti(A-HC-H) samples (1 − 2N) while it is delayed for Ti64(A-Ca-H-W) and Ti64(HF-H_2O_2) samples (4–5 N). The damage rapidly increases (substrate completely exposed at 3 N of applied load) for Ti64(A-H) and Ti(A-HC-H) samples while it occurs around 9 N for Ti64(HF-H_2O_2) and around 21 N for Ti64(A-Ca-H-W) sample.

Comparing the profiles along the scratch channel (Fig. 3e), the first difference is the higher penetration depth of sample Ti(A-HC-H) respect to the others. This can be due to the lower substrate hardness of pure titanium (280 HV) respect to Ti-6Al-4 V alloy (349 HV). The effect of the lower substrate hardness can be noticed also in picture 3f, where not only a higher depth was found for Ti(A-HC-H), but also a higher deformation along the scratch channel.

In the case of the bioactive glass, the interpretation of the results is a bit different, in fact in this case a surface layer is not present and the measurement can be considered as an evaluation of surface hardness/resistance to scratches. BG sample is almost undamaged up to 4 N, then some small cracks appears, but a significant surface damage with evident enlargement of the scratch track can be observed about starting from 12 N.

3.3. The substrate–bioactive surface layer interface: the micro scratch test

The critical scratch loads of the samples were also examined by micro scratch test as shown in Fig. 4. In this test, a stylus having smaller diameter (5 μm, Fig. 4c) compared to macro scratch test (200 μm, Fig. 3d) was used. Further, the stylus was loaded with amplitude of 100 μm that is in contrast to the linear movement of macro scratch test. Because of these differences in the test conditions, the obtained values of complete failure (critical loads of first damage are not detectable by this test) are expected to be different from those obtained by the macro scratch test. Ti64(A-Ca-H-W) showed the highest critical scratch load of about 70 mN analogously to the previous result. Ti64(A-H) and Ti(A-HC-H) showed a similar value (about 50 mN) of critical scratch load, analogously to the previous results, that is higher than the value of Ti64(HF-H_2O_2) (about 10 mN): this surface is quite more sensitive to the micro scratch than to the macro one. Surface fracture was observed on BG sample at about 70 mN.

3.4. The substrate–bioactive surface layer interface and the hydroxyapatite-bioactive surface layer interface: the Zeta potential titration curves of the as-prepared and soaked samples

As first, zeta potential applied to bulk materials is an interesting technique to evaluate the charge and reactivity of the functional groups of the as-prepared sample surfaces, which affects their bioactivity mechanism as investigated in [25]. Moreover, it is a useful method to evaluate the surface changing during soaking in SBF because of adsorption of ions and the chemical/mechanical stability of the formed hydroxyapatite layer considering that both pH changing and liquid flux is applied.

The zeta potential titrations curves and values of the delta of the gap between the two specimens during the measurement for the as-prepared and SBF soaked samples (1-7-28 days) are reported in Fig. 5.

A detailed description of the zeta potential titration curves of the as-prepared samples has been already reported in [25] and it is here briefly summarized. In the case of all titanium samples (Fig. 5 a-d), the standard deviation of the zeta potential values is low (in the range

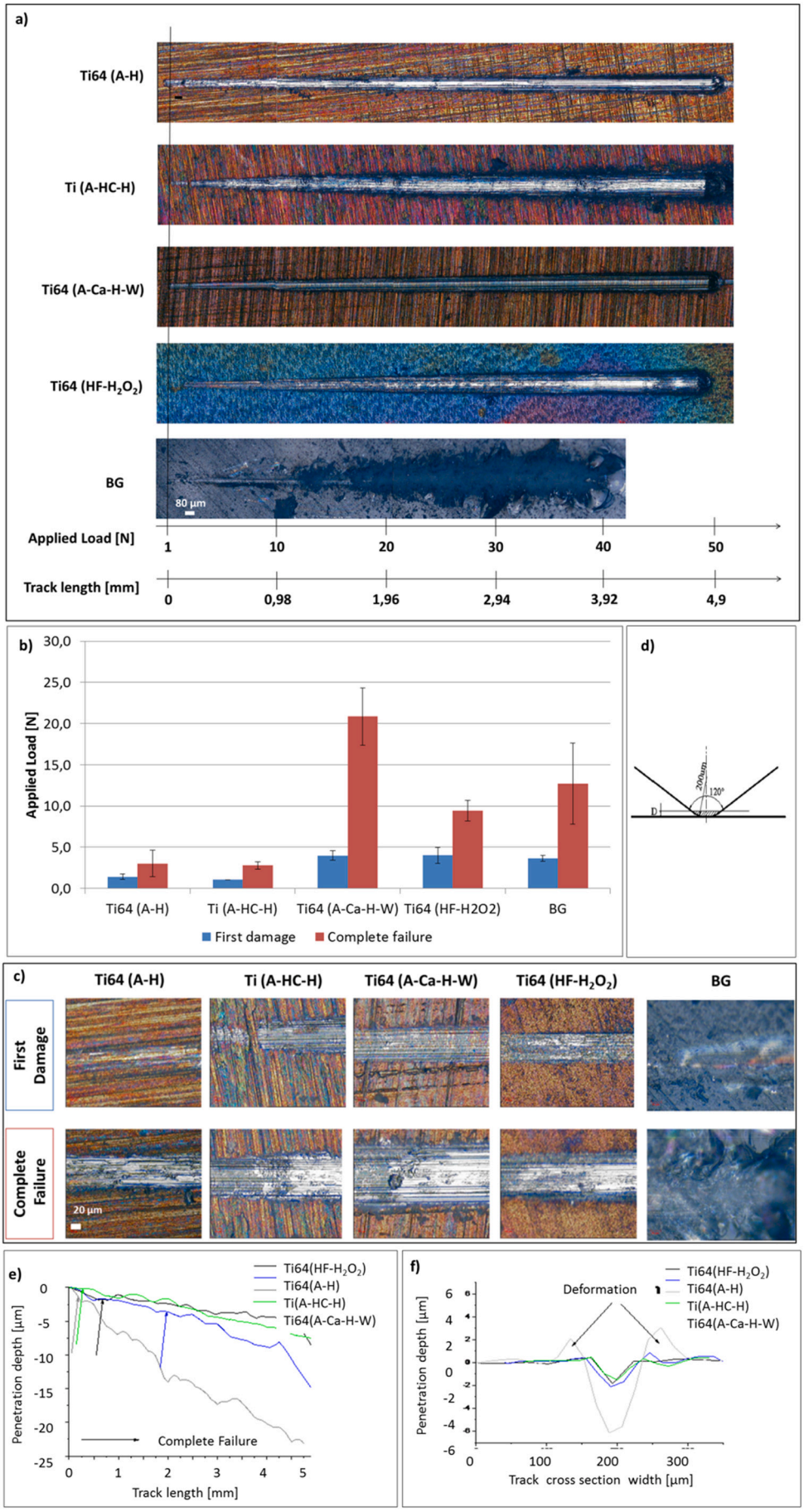

(caption on next page)

Fig. 3. Macro scratch test. a) Scratch tracks (optical observation, 5×), b) Comparison of the critical loads values, c) details of the tracks at the critical loads (optical observation, 20×), d) scheme of the macro scratch indenter, e) 2D profile along scratch track, e) bi-dimensional profile at 1 mm after the beginning of the scratch track.

0.1–1 mV) and constant during the measurement, no significant (higher than 5 μm) delta of the gap between the two specimens was registered. The standard deviation of the zeta potential values is related to the stability or reactivity of the surface during the measurement, while the delta of the gap between the specimens is related to the stability or detachment of the surface layers during the test. As-prepared BG (Fig. 5e) has some reactivity in the basic range (standard deviation of the zeta potential values higher than 1 mV at pH higher than 8).

Concerning the presence of functional groups on the surface of the as-prepared samples, Ti(A-HC-H) (Fig. 5b, IEP = 5.6) has a positive surface charge at pH lower than 5.6 and OH groups with a strong basic behavior completely protonated at a pH lower than 3.5; it shows also acidic OH groups without a specific acidic strength which are not completely deprotonated at a specific pH value. Ti64(HF-H_2O_2) (Fig. 5d, IEP ≈ 2) and BG (Fig. 5e, IEP = 3.1) have OH groups with a strong acidic strength and basic OH groups with a weak basic strength. Ti64(A-H) (Fig. 5a, IEP = 3.5) has OH groups without a specific acidic strength. On Ti64(A-Ca-H-W) (Fig. 5c, IEP = 3.8), even if OH groups are exposed on the surface, they are too weak to give an acid or basic reaction within the explored pH range.

After soaking in SBF, the zeta potential titration curves are changed vs the as-prepared samples, indicating a change in the surface chemistry and charge of the materials during soaking in SBF.

After 1 and 7 days of soaking in SBF, IEPs for Ti64(A-H) (Fig. 5a), Ti (A-HC-H) (Fig. 5b) and Ti64(A-Ca-H-W), (Fig. 5c) is shifted towards lower values with respect to the as-prepared materials and an evident plateau is observed in the basic region according to the presence of OH groups with high acid strength. On the other hand, an opposite shift (towards higher values) is observed for Ti64(HF-H_2O_2) (Fig. 5d) and BG (Fig. 5e). The plateau in the basic region is present after soaking in SBF, but it was observed also for the as-prepared samples, in this case.

After 28 days of soaking, IEP moves towards right for all samples, except for Ti(A-HC-H) (Fig. 5b). The IEP moves to values around 4.5–4.8 (a value close to the one reported in literature for hydroxyapatite [37]), for Ti64(A-H) (Fig. 5a), Ti64(A-Ca-H-W) (Fig. 5c) and Ti64(HF-H_2O_2) (Fig. 5d) while a more limited shift (from 3.1 to 3.3) was observed for BG (Fig. 5e). A significant plateau in the basic region in the range of −13/−33 mV is observable on all samples soaked for 28 days.

Concerning the standard deviation of the soaked samples, a significant increase in the standard deviation (values around 5–10 mV and even higher) can be observed in some situations. For Ti64(A-H) (Fig. 5a) after 1 and 7 days of soaking in SBF, there is a higher standard deviation (up to 2 mV) below pH 4. For Ti64(A-H) (Fig. 5a) after

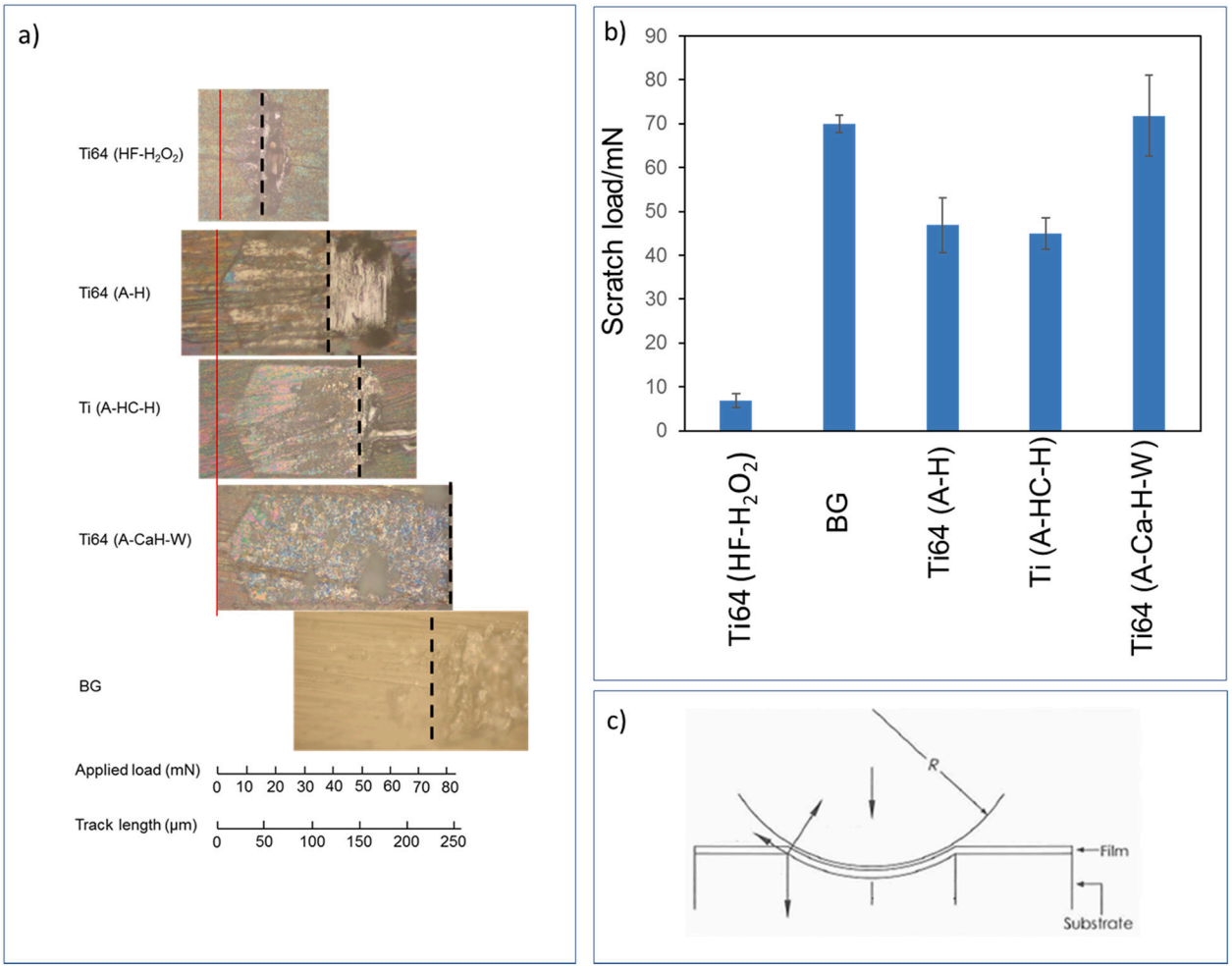

Fig. 4. Micro scratch test: a) optical images of the micro-scratch tracks (dotted lines correspond to complete failure), b) values of the critical scratch loads (at complete failure) registered for the different samples, c) scheme of the micro-scratch indenter.

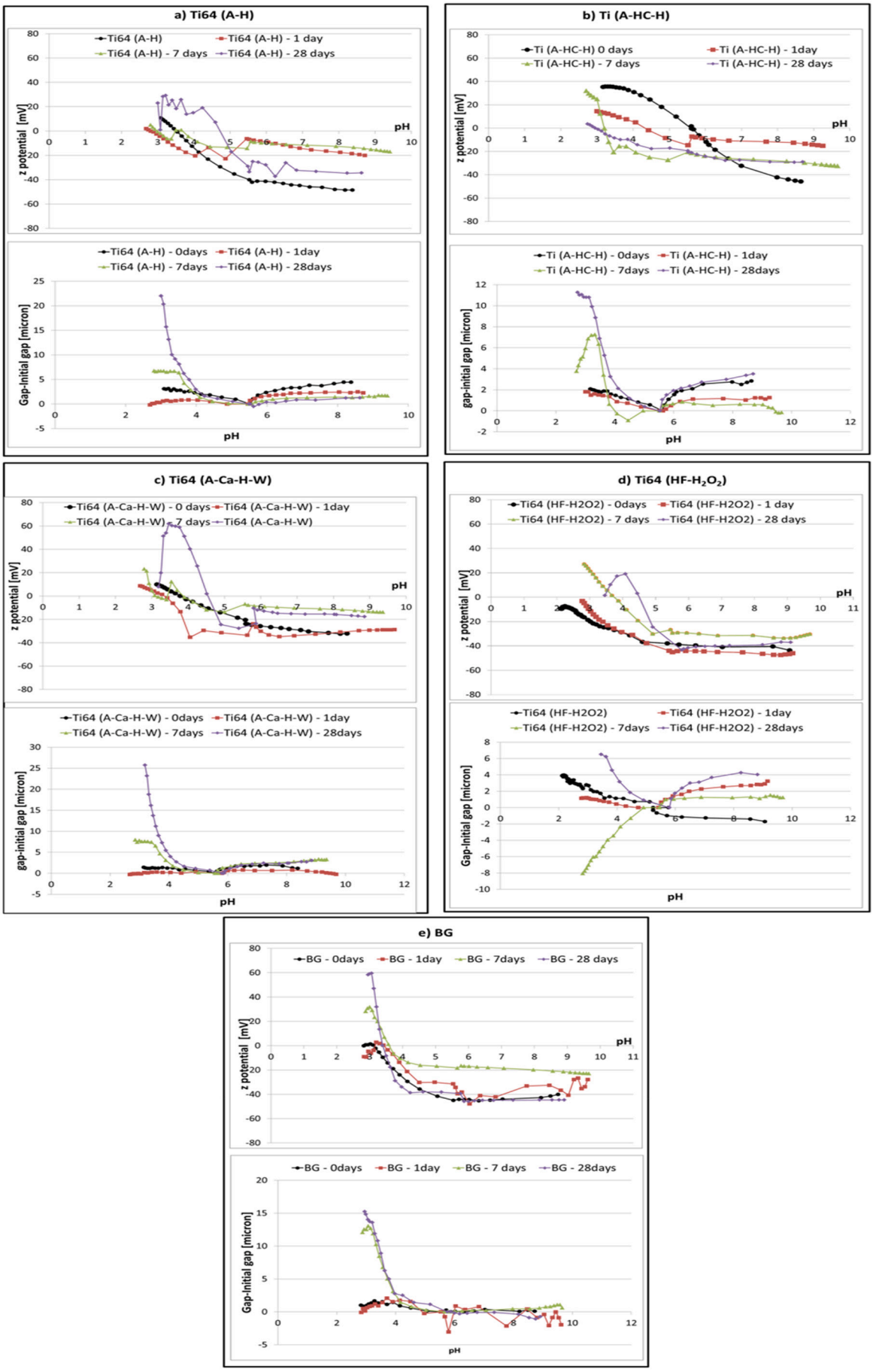

(caption on next page)

Fig. 5. Zeta potential titration curves and gap variations (measured gap-initial gap) for a) Ti64(A-H), b) Ti(A-HC-H), c) Ti64(A-Ca-H-W), d) Ti64(HF-H_2O_2) and e) BG.

28 days of soaking, a first increase in the SD (up to 25 mV) can be evidenced in the basic range, followed by a more evident increase (up to 66 mV) in the acidic range (below pH 3.7). For Ti(A-HC-H) (Fig. 5b), the SD is above 1 mV on all soaked samples with an increase (up to 8 mV) on the samples soaked for 7 and 28 days below pH 3.8. A high standard deviation (up to 10 mV) in the acidic range can be noted for Ti64(A-Ca-H-W) (Fig. 5c) at all the soaking times, but it is more pronounced (> 10 mV) for the samples soaked for 28 days at pH below 4.8. Concerning Ti64(HF-H_2O_2) (Fig. 5d), a peak in the SD value (up to 6 mV) can be recorded below pH 4.5 only for the sample soaked for 28 days. Finally, BG (Fig. 5e) shows a very high SD (around 14 mV) in the basic range for the sample soaked for 1 day and in the acidic range for all soaked samples.

Looking at the gap variation during the measurements, it can be observed that the distance between the two samples is almost constant in the basic range for all materials. On the other hand, an appreciable increase in the gap width (higher than 5 μm) can be observed in the acidic range (mainly below pH 3.9) for all samples soaked for 7 and 28 days, except of Ti64(HF-H_2O_2).

3.5. Bioactivity: FESEM observations

The cross sections and top view FESEM images of the surfaces before and after soaking in SBF (1, 7 and 28 days) are reported in Figs. 6–7 in order to evaluate the growth and coverage degree of the surfaces by the formed hydroxyapatite layer.

A continuous hydroxyapatite layer can be observed on Ti64(A-H), Ti (A-HC-H), Ti64(A-Ca-H-W) and BG from the first days of soaking in SBF and it grows up to 28 days, reaching 11 μm for Ti64(A-H) and BG (Fig. 6). Hydroxyapatite growth is slower on Ti64(HF-H_2O_2), as previously reported by the authors [25], but it reaches an almost complete coverage and relevant thickness (6 μm, Fig. 6) after 28 days of soaking. The hydroxyapatite layer grows on a bioactive surface layer on the samples: it is the surface oxide for the metallic samples while a silica gel layer is formed on the bioactive glass surface during soaking in SBF before the formation of hydroxyapatite, as previously reported by the authors [25].

Looking at the top views (Fig. 7), a nanoporous surface morphology can be observed on all titanium based materials, while a smooth one (except from polishing tracks) characterizes BG, as previously reported by the authors [25].

A continuous layer of hydroxyapatite covers the whole surface of Ti64(A-H), Ti(A-HC-H), Ti64(A-Ca-H-W) and BG from 1 day of soaking on (Fig. 7). The hydroxyapatite morphology is globular on the titanium surfaces up to 7 days, while it is more continuous for the glass one since the first day and becomes more similar for the titanium substrates after 28 days. As already observed on the cross-sections, the bioactivity of Ti64(HF-H_2O_2) is slower and no hydroxyapatite is clearly observable by FESEM up to 7 days soaking in SBF (Fig. 7). After 28 days, a globular like hydroxyapatite covers large part of the surface, even if, differently from the others materials, the substrate is still visible in some zones.

3.6. The substrate-bioactive surface layer interface and the hydroxyapatite-bioactive surface layer interfaces: FESEM observation of the samples after the zeta potential measurements

The top view FESEM images of the samples used for the zeta potential measurements are reported in Fig. 8; the test was applied both to the as-prepared and soaked samples (in SBF for 1, 7 and 28 days). This observation is useful for a better understanding of the zeta potential titration curves and in order to evaluate if the surface bioactive layers (in the case of the as-prepared samples) or the formed hydroxyapatite layers (in the case of the samples soaked in SBF) are chemically/mechanically stable or not, that means if pH changing and the liquid flux occurring during the zeta potential titration measurements are able to remove them.

No evident alteration of the surface morphology can be detected on the as-prepared samples after the zeta potential measurement.

On the other hand, significant modifications occur on the soaked samples and a different behavior can be evidenced for the different surfaces. In particular, hydroxyapatite is no more visible after the zeta potential titration measurement on all samples except for Ti64(HF-H_2O_2) after 28 days of soaking and BG after 1 day of soaking in SBF. Hydroxyapatite on these samples is highlighted by red boxes in Fig. 7 and its composition confirmed by the EDS analyses (not reported). For Ti64(A-H) and Ti64(A-Ca-H-W) soaked for 1 and 7 days, the surface appearance and chemical composition (EDS) after the zeta potential titration measurement is analogous to the one of the as-prepared samples, with the complete absence of hydroxyapatite. The EDS analyses (not reported) confirm that the oxide layer composition is close to that of the as-prepared samples, with the presence of Na and Ca on Ti64(A-H) and Ti64(A-Ca-H-W), respectively. After 28 days of soaking in SBF and the zeta potential titration measurement, in addition to the complete disappearance of the hydroxyapatite layer, a detachment of the porous oxide layer occurs on Ti64(A-H) and Ti64(A-Ca-H-W). For Ti(A-HC-H), the detachment of the surface porous oxide layer is already visible on the sample soaked for 1 day. When the detachment of the porous oxide layer occurs, for all cited samples, a compact oxide layer (distinguishable from the metal by the high value of oxygen detected by EDS) is observable below the porous one on the majority area of the sample.

In the case of Ti64(HF-H_2O_2), no detachment of the oxide layer can be observed upon zeta potential titration measurements even after soaking in SBF for 28 days and, as already mentioned, hydroxyapatite is still observable.

As far as the bioactive glass is concerned, as observed above, a certain amount of hydroxyapatite is still visible on the sample soaked for 1 day and used for the zeta potential titration measurement, while it is absent on the samples soaked for 7 and 28 days. In this case, a layer of cracked silica gel is visible on the soaked samples used for the zeta potential titration measurement.

3.7. FTIR chemical imaging

FTIR chemical imaging analysis was performed on the different materials after 7 days and 28 days of soaking in SBF in order to investigate the evolution of hydroxyapatite formation. FTIR allows monitoring the progressive growth of the apatite crystals from simulated and natural body fluids [38]. The absorption frequency of the peak related to the phosphate group gives information on crystallinity of the deposited material. Moreover, it is possible to determine the carbonatation degree as well as to distinguish between two types of carbonatation (A and B).

3.7.1. Samples soaked for 7 days

The optical analysis of Ti(A-HC-H), Ti64(A-H), Ti64(A-Ca-H-W) and BG shows a layer likely attributable to hydroxyapatite (Fig. 9 a, e, I, m). Spectra analysis shows the presence of absorption bands in the regions of absorbed water, carbonates and phosphates (Fig. 9 d, h, l, p).

In the carbonate region an evident band is observed at about 1415 cm^{-1}, with a shoulder for Ti(A-HC-H), Ti64(A-H), Ti64(A-Ca-H-W) and BG at around 1455 cm^{-1}. The combination of the absorption bands at 1415 cm^{-1} and 1455 cm^{-1}, as well as at 870 cm^{-1}, proves for all samples the substitution B-type of the phosphate groups with the

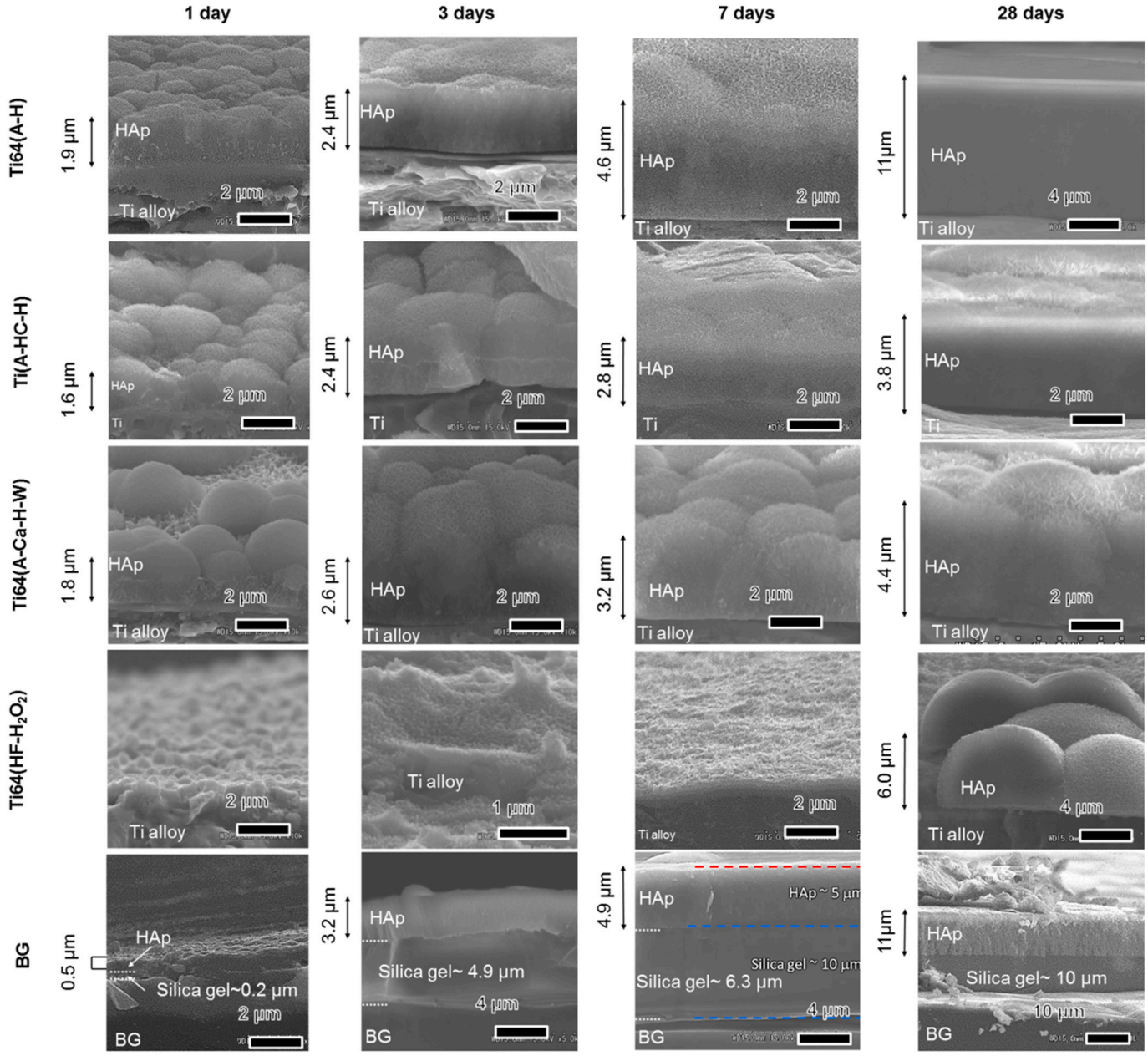

Fig. 6. Cross sectional SEM images on bioactive Titanium samples and glass, after soaking in SBF for different periods.

carbonate groups in the hydroxyapatite crystal lattice. The samples Ti64(A-Ca-H-W) and BG, that at 1 day showed an A-B type substitution [25], seem to move towards a prevalent B-type substitution after 7 days. The obtained data are reported in Table 1.

In the spectra of all samples, it is also evident a broad band in the range 3600-2600 cm^{-1} due to absorbed water and a very small peak at 3750 cm^{-1}. According to some authors, this weak peak can be attributed to the stretching vibration of the OH^- ions in the inner lattice of no-stoichiometric hydroxyapatite [39,40]. It is reported in the literature that the vibration at 3560 cm^{-1} is due to the OH- in the channels of the crystals, while it moves to around 3750 cm^{-1} when it is due to the OH- in the inner of the crystals: these ions are mainly affected by the interaction with calcium, responsible for the shift of the frequency towards higher values. Moreover, with increasing immersion time, the phosphate bands become sharper thus indicating a growth of more crystalline hydroxyapatite. After 7 days, the typical bands of the phosphates are present: n_3 P-O asymmetric stretching at 1100-900 cm^{-1} and a shoulder of n_1 P-O asymmetric stretching at 960 cm^{-1}. In the phosphate region, the band due to the PO_4 stretching vibration is present for all samples examined, in particular an intense band at 1020 cm^{-1} is observed for the titanium samples, while the band of BG sample is moved to lower frequencies around 1010 cm^{-1}. This band shows also a shoulder that in second derivative appears at 950 cm^{-1} (Fig. 9, c, g, k, o). The simultaneous presence of these two absorption bands is indicative of non-stoichiometric crystalline hydroxyapatite. The possible shift of the peaks at 1020 cm^{-1} and 1010 cm^{-1} compared to those of stoichiometric hydroxyapatite [25] at 1040 cm^{-1}, is due to the presence of carbonates and crystal imperfections. Moreover, in all samples is evident a small signal at 1180 cm^{-1} associated to the acid phosphates groups. Differences in phosphate distribution can influence biocompatibility of hydroxyapatite. Chemical map in function of the phosphate band intensity was performed to evaluate the presence of the phosphate bands in the mapped areas. The samples after 7 days of soaking in SBF showed high values of band intensity (red and green zones) for all mapped surfaces. This indicates a good homogeneous presence of the phosphates over the entire observed surfaces (Fig. 9, b,

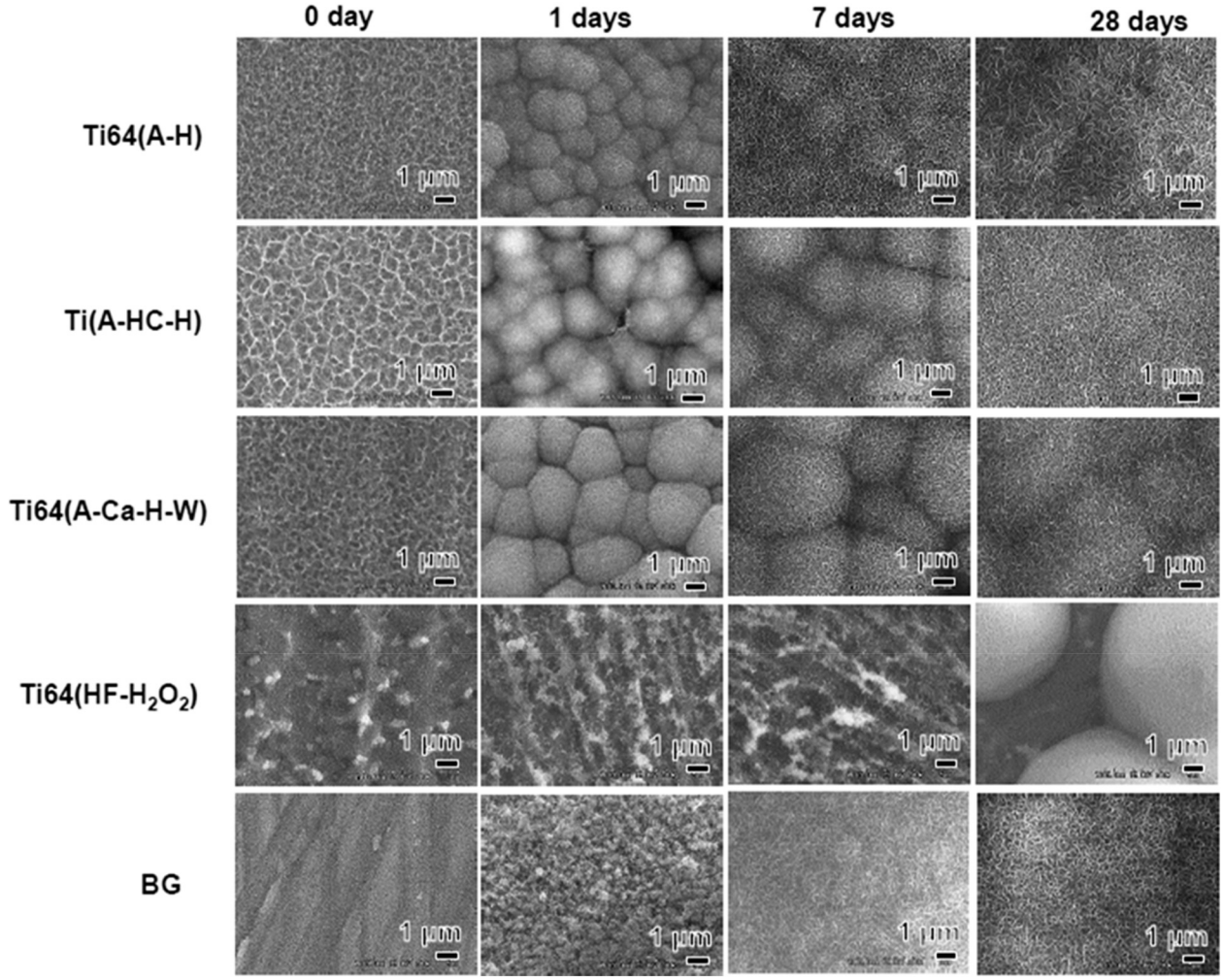

Fig. 7. Top view FESEM images of the surfaces before and after soaking in SBF (1, 7 and 28 days).

f, j, n).

The Ti64(HF-H_2O_2) sample, that after 1 day of soaking in SBF showed a lower development of calcium phosphate on the surface than on the other surfaces, after 7 days of soaking shows, in addition to the bands at 1516 cm^{-1} and at 1170 cm^{-1} (acid phosphate), a small peak, detectable only in some zones, at 1006 cm^{-1} related to an initial deposition of the phosphate groups (data not shown).

The degree of carbonation of the phosphate matrix on the surface of the samples after 7 days of soaking in SBF was obtained by calculating the ratio (R) between the carbonate (numerator) and phosphate (denominator) contribution using an area-based method [25,41]. The chemical maps, as a function of ratio band, showed a variability in the maximum and minimum R value (R_{max} and R_{min}) for all samples (Table 1). Ti(A-HC-H) and Ti64(A-H) showed R values of 2–3%, on the contrary for Ti64(A-Ca-H-W) and BG the R values resulted slightly higher of 3–4%.

3.7.2. Samples soaked for 28 days

The analysis of spectra acquired from the maps of samples soaked for 28 days (Fig. 10) do not show differences in the carbonate region if compared with analysis of spectra for the samples soaked for 7 days (Fig. 9). In all samples the bands at 1455 cm^{-1}, 1418 cm^{-1} and 870 cm^{-1} are present indicating a prevalent type-B substitution (Fig. 10 d, h, l, t). The region of phosphates results characterized by a clear peak between 1020 cm^{-1} and 1015 cm^{-1}.

A broad band in the range 3600–2600 cm^{-1}, due to absorbed water, and a little peak at 1180 cm^{-1}, associated to acid phosphate, are also present in these samples as observed after 7 days of soaking in SBF, even if at lower intensity. The analysis in second derivative shows a certain degree of variability in the region of ν_3 PO_4 respect to the samples soaked for 7 days (Fig. 10 c, g, k, s). The band corresponding to ν_1 PO_4 is also present in all samples. Chemical map in function of phosphate band intensity performed on samples soaked for 28 days are reported in Fig. 10 b, f, j, r. Although the whole surface shows the presence of phosphates, numerous areas with lower band intensity values (blue zones), respect to samples soaked for 7 days, are observed. This result could be related to a fragmentation observable from the optical images (Fig. 10 a, e, I, p), attributable to a higher fragility of the layer that renders more irregular the sample surface.

The comparison of ratio band reported in Table 1 among samples after soaking in SBF for 7 and 28 days do not show substantial variations for Ti64(A-H) and Ti(A-HC-H). On the contrary, Ti64(A-Ca-H-W) and BG samples soaked for 28 days show values of the ratio band lower respect to those registered after soaking in SBF for 7 days, indicating a lower carbonation degree. It is interesting to note how the spectra acquired in areas with minimum and maximum band ratio are different in the region of absorbed water (3600–2600 cm^{-1}). In particular, where the ratio is lower, this band is very small or even disappeared for all examined samples.

After 28 days of soaking in SBF, the analysis of Ti64(HF-H_2O_2) sample shows some areas of its surface characterized by spectra having bands at 1455 cm^{-1}, 1418 cm^{-1} and 870 cm^{-1} indicative of a B-type substitution, and a band at 1015 cm^{-1} due to PO_4 stretching vibration, as confirmed by the high correlation value with phosphate groups

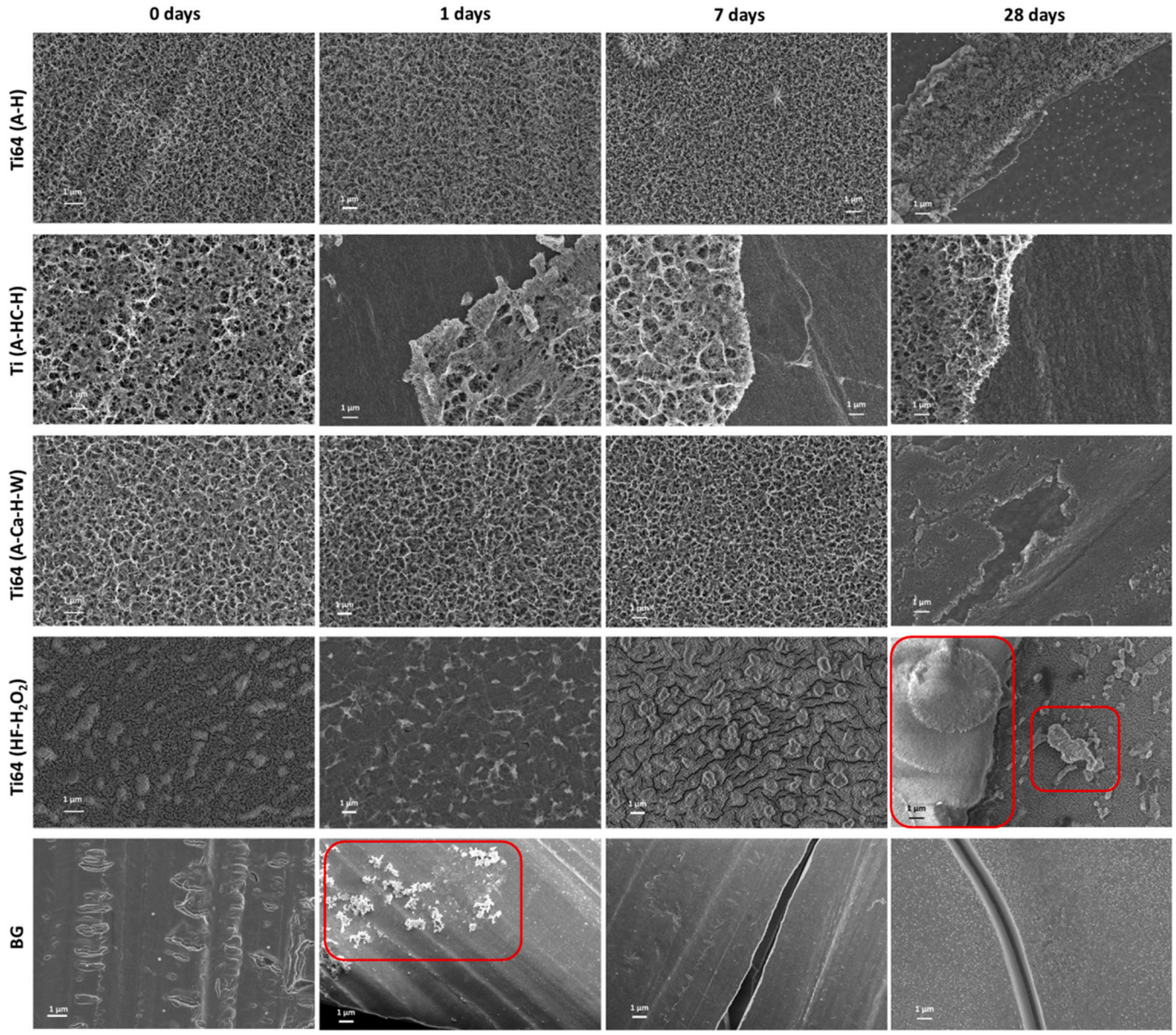

Fig. 8. Top view FESEM images of the surfaces before and after SBF soaking (1, 7 and 28 days) after zeta potential measurements.

(Fig. 10 m, n, o, p). However, some areas where acid phosphate is still present are indicative of an incomplete coverage of titanium surface.

The degree of carbonation of the phosphate matrix on the surface of the samples soaked for 28 days showed slightly higher values for Ti(A-HC-H) and Ti64(A-H) on the contrary for Ti64(A-Ca-H-W) and BG a significant reduction of carbonation degree was observed (Table 1).

4. Discussion

Investigation of hydroxyapatite formation on bioactive materials is usually focused on the kinetics or the mechanism of nucleation and growth of the hydroxyapatite crystals from the calcium and phosphate ions in SBF. Differently, in this paper, the focus is on maturation of hydroxyapatite, as well as on the mechanical and chemical stability of the interfaces of a bioactive material, considering their relevance in an implant with high bone bonding ability. In fact, the mechanical stability of the surfaces and interfaces of a bone implant are relevant because of the friction load applied during implantation and micro-sliding occurring during the implant life with respect to bone or cement [42]. On the other side, the chemical stability is of great interest considering that, even if the physiological pH is constant at 7.4, inflammation phenomena occur early after implantation with wide pH variation eventually down to pH 4 [43]. Moreover, the implant surfaces are in contact with the biological fluids and tissues for all the implant life and should maintain their characteristics in this peculiar “working conditions”.

Two different classes of bioactive materials are considered and compared in this paper: titanium based materials, chemically (and eventually thermally) treated, and a bioactive glass. Ti was used as a substrate in the case of Ti(A-HC-H) while Ti6Al4V was used for Ti64(A-H), Ti64(A-Ca-H-W) and Ti64(HF-H_2O_2) according to the literature [27–29]. The difference between c.p. Ti and Ti6Al4V alloy as substrates can be considered as negligible for the purpose of this research, as explained below. The bioactive glass selected for this work is a state-of-the-art silica-based glass obtained by the melt and quenching route. Its composition belongs to the class of 45S5 Bioglass®, modified for the different proportion between the network former and modifier oxides, as well as for the addition of small amount of B_2O_3 and Al_2O_3 to regulate reactivity, as reported in previous works [26,44,45].

In a previous work [25], the authors concluded that when the hydroxyapatite precipitation mechanism is based both on ion exchange

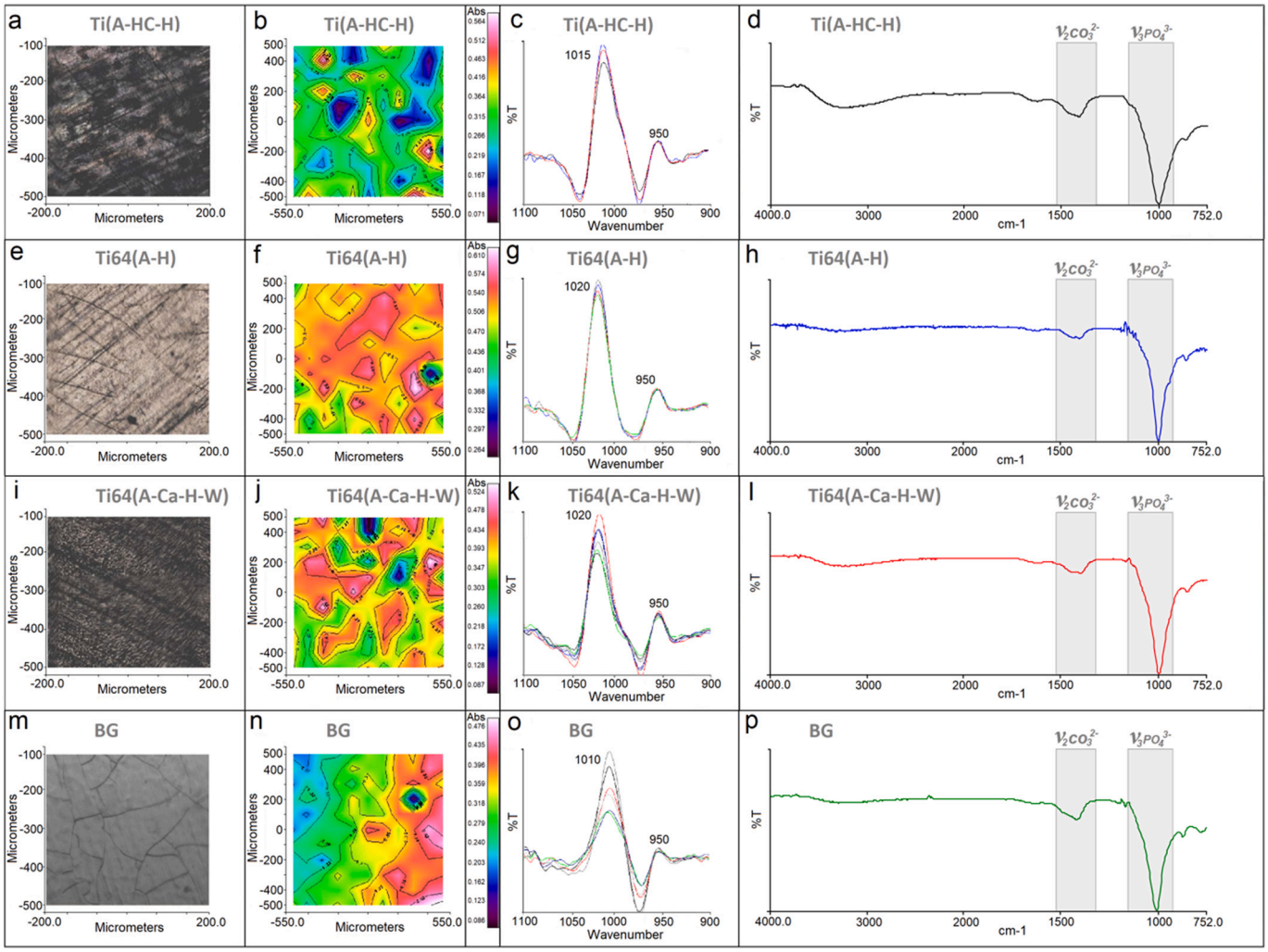

Fig. 9. FTIR Chemical Imaging: optical images (a, e, i, m), chemical map in function of phosphate band intensity (b, f, j, m); second derivative of phosphate band (c, g, k, o); spectra (d, h, l, p) of Ti(A-HC-H), Ti64(A–H), Ti64(A-Ca-H-W), BG samples soaked for 7 days, respectively.

Table 1
FTIR data of the samples after soaking in SBF for 7 and 28 days.

Sample	ν_3 CO_3 (cm^{-1})		ν_2 CO_3 (cm^{-1})	ν_3 PO_4 (cm^{-1})	ν_1 PO_4 (cm^{-1})	Ratio band ν_3 CO_3 /ν_3 PO_4 R_{max}- R_{min}	Percentage of carbonation wt% CO_3 R_{max}- R_{min}
Ti(A-HC-H) 7 day SBF	1450	1417	870	1020	960	0.10–0.07	2.9–2.1
Ti(A-HC-H) 28 day SBF	1460	1420	870	1020	960	0.12–0.07	3.5–2.1
Ti64(A-H) 7 day SBF	1455	1415	870	1020	960	0.09–0.07	2.7–2.1
Ti64(A-H) 28 day SBF	1455	1418	870	1015	960	0.11–0.09	3.2–2.7
Ti64(A-Ca-H-W) 7 day SBF	1455	1419	870	1020	960	0.12–0.09	3.5–2.7
Ti64(A-Ca-H-W) 28 day SBF	1458	1418	870	1020	960	0.09–0.06	2.7–1.8
BG 7 day SBF	1455	1418	870	1010	960	0.14–0.12	4.0–3.5
BG 28 day SBF	1455	1418	870	1015	960	0.09–0.08	2.7–2.4

and electrostatic attraction of ions by deprotonated OH groups, it results in very fast kinetics of precipitation at short time (1 day): the fastest is BG, with exchange of both Na^+ and Ca^{2+}, followed by Ti64(A-H), with exchange of Na^+. Ti64(A-Ca-H-W) has slower kinetics of hydroxyapatite precipitation because the mechanism is based on the ion exchange of Ca^{2+} and no contribution comes from the deprotonated surface OH groups. On the other side, the mechanism based only on the surface charge effect, such as in the case of Ti64(HF-H_2O_2), is the slowest even if abundant and strongly reactive functional groups are present on the surface. The occurrence of a micro-environment effect, in the case of Ti(A-HC-H), is able to enhance kinetics of hydroxyapatite precipitation based on a net surface charge up to be comparable with Ti64(A-Ca-H-W). Concerning the type of hydroxyapatite deposition, the presence of hydroxyapatite much closer to the biological one (type B, less crystalline and with highly carbonate degree) is earlier developed on Ti(A-HC-H) and Ti64(A-H), while Ti64(A-Ca-H-W) and BG induce precipitation of hydroxyapatite of type A-B, with higher degree of crystallinity and lower of carbonation.

In the case of the titanium substrates, the interfaces of interest are the one between hydroxyapatite and the surface oxide layer and the one between the surface oxide layer and the metal substrate. On some samples, the surface oxide layer is formed by several oxides, as

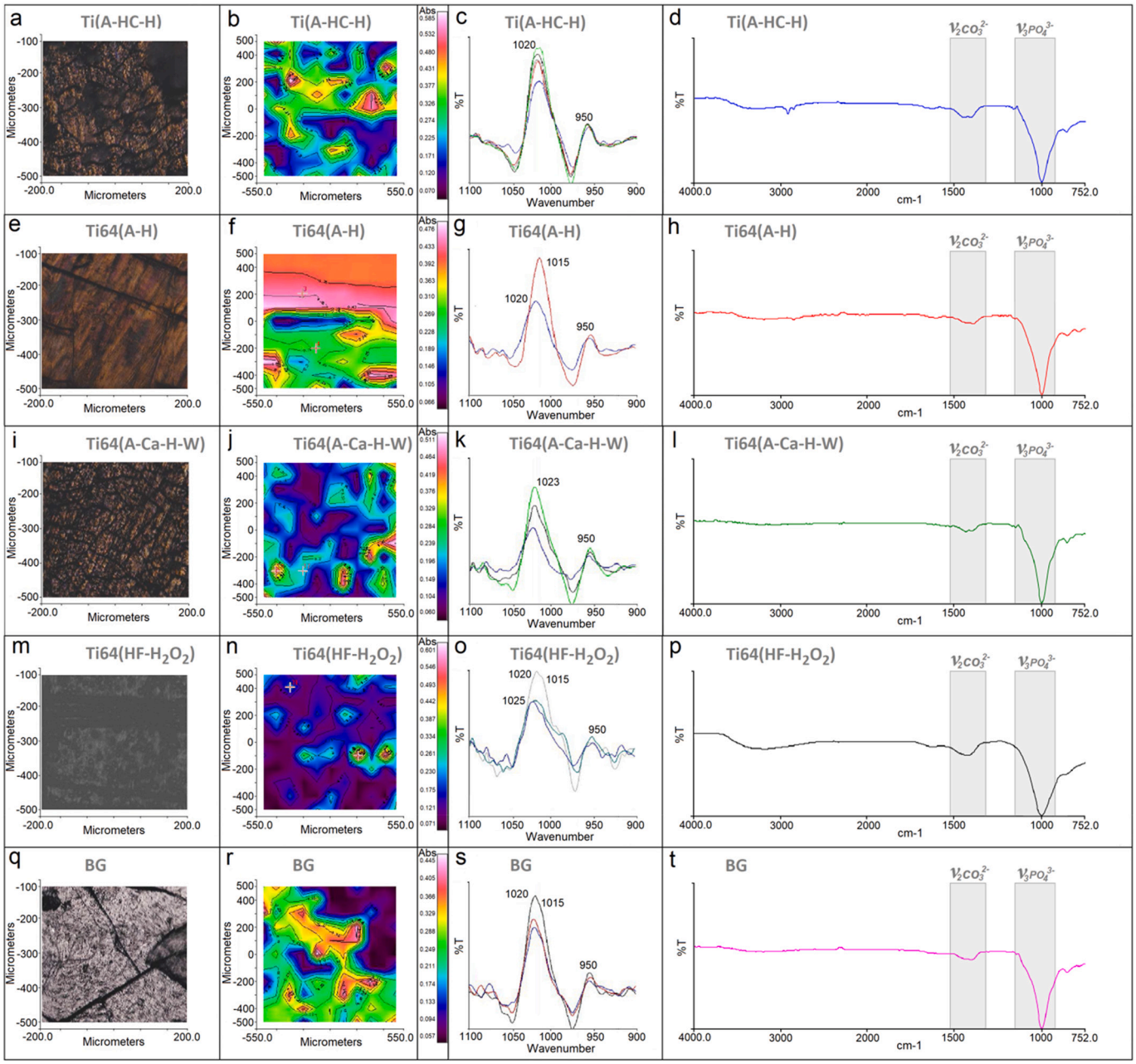

Fig. 10. FTIR Chemical Imaging: optical images (a, e, i, m, q), chemical map in function of phosphate band intensity (b, f, j, n, r); second derivative of phosphate band (c, g, k, o, s); spectra (d, h, l, p, t) of Ti(A-HC-H), Ti64(A–H), Ti64(A-Ca-H-W), Ti64(HF-H_2O_2), BG samples soaked for 28 days, respectively.

evidenced by Raman analyses, and, according to previous works, by a compact inner and an outermost porous layer. In the case of Ti64(A-H) [46] and Ti64(A-Ca-H-W) [29] the outermost layer can be respectively attributed to sodium or calcium titanate, while the inner oxide layer can be respectively attributed to rutile or anatase. Ti(A-HC-H) is mainly covered by anatase [47], with a porous morphology in the outermost layer, and Ti64(HF-H_2O_2) has a single thin surface layer of $H_2Ti_3O_7$. In the case of the bioactive glass, there is a silica gel layer, formed during the soaking in SBF [25], acting as a bioactive surface layer.

The mechanical stability of the interface between the bioactive surface layer and the substrate was explored by scratch measurements in different conditions of applied load and scratch tip shape.

Macro scratch test (loads up to tens of N and bigger tip diameter, 200 μm) and micro scratch tests (loads up to 100 mN and smaller tip diameter, 5 μm) were performed and compared in order to better understand the mechanical behavior of the interface between the bioactive surface layer and the substrate.

As far as macro scratch resistance is concerned, continuous ductile perforation was found for all tested samples with a metal substrate. The indenter penetration is higher for Ti(A-HC-H) sample, with evident signs of deformation, due to the softer nature of the substrate (as evidenced in the results section), however it seems that the differences in the critical loads are not only affected by the substrate deformation. In fact, even if the indenter penetration is driven by the substrate hardness, significant differences in the critical loads can be observed among the samples of the same substrate. Moreover, despite of the differences in the bioactive surface oxide layer thickness (1.2 μm for Ti(A-HC-H), 1.6 μm for Ti64(A-H) and Ti64(A-Ca-H-W) and 400 nm for Ti64(HF-H_2O_2) [25]) the critical loads are not grouped on the basis of the thickness. So, the effect of the substrate nature and of the coating thickness should be taken into account, but they are not the main factors affecting the macro-scratch results which can be considered

representative of the difference in the scratch resistance of the oxide bioactive layers. Comparing the second critical load (complete failure), Ti64(A-Ca-H-W) sample showed a higher scratch resistance, followed by Ti64(HF-H_2O_2) and Ti64(A-H), finally Ti(A-HC-H). The complete failure load of BG is close to the one of Ti64(HF-H_2O_2), but it is related to a fragile failure (typical of glasses).

Looking at micro scratch results the highest critical load is reached by Ti64(A-Ca-H-W), analogously to the macro scratch case, on the other hand, in this conditions Ti64(HF-H_2O_2) presented the lowest failure load, evidencing a more pronounced sensitivity to localized loads. Ti64(A-H) and Ti(A-HC-H) showed an intermediate behavior, indicating a more pronounced sensitivity to high and distributed stresses (macro scratch condition) of the last one. BG showed a failure load close to the one of Ti64(A-Ca-H-W).

As far as Ti64(HF-H_2O_2), a different behavior was found between micro and macro scratch concerning the second critical load. Indeed, while for macro scratch this layer showed an intermediate critical load failure between Ti64(A-H) and Ti(A-HC-H) and Ti64(A-Ca-H-W),which support the resistance of this surface to implantation friction, previously reported by the authors [6], for micro scratch it showed the lowest value.

As mentioned in [48], an indenter with a smaller tip (sharper) can generate over the surface a higher stress. With low indenter radius, the stress is more located in the coating, while increasing the radius, the stress moves to the interface. The sharper indenter radius, together with the low thickness (400 nm) can be an influence on coating Ti64(HF-H_2O_2) adhesion.

FTIR chemical imaging was used for the investigation of the maturation of hydroxyapatite along 28 days.

Concerning evaluation of carbonation degree, the comparison of the results obtained for soaking of 7 and 28 days, respect to those obtained for soaking of 1 day [25], shows a reduction of carbonation degree for all samples with increasing the soaking time in SBF. This result is particularly significant in the case of Ti64(A-Ca-H-W) and BG samples. FTIR Chemical Imaging analysis shows that hydroxyapatite on the samples surface contains carbonates in the range of the biological hydroxyapatites of 2–8% by weight (depending on the source, species, and age). For all samples, a B-type substitution was observed, in particular there is an evolution towards the B type for Ti64(A-Ca-H-W) and BG samples that at 1 day showed an A-B type substitution. B-type hydroxyapatite is the preferred form of biological-like hydroxyapatites because it promotes the formation of biominerals with improved mechanical and biological properties, compared to stoichiometric hydroxyapatite. The biocompatibility of the carbonated hydroxyapatite can be attributed to the tendency of the carbonate to reduce the crystallinity within the hydroxyapatite structure, thus increasing its solubility that favors bone re-formation or turnover.

The results of the FTIR analysis associate the material deposited on the surfaces of the samples after soaking in SBF to a non stechiometric biological hydroxyapatite [49,50]. The presence of sharper phosphate bands and a more uniform distribution of the phosphates groups for the samples soaked for 7 days evidence, for Ti(A-HC-H), Ti64(A-H), Ti64(A-Ca-H-W) and BG samples, a more homogeneous hydroxyapatite coverage at this experimental time (compared to the 28 days one). The less homogeneous coverage of hydroxyapatite on these surfaces after 28 days soaking in SBF can be partially attributed to an experimental artifact. In fact, the thick hydroxyapatite layers (up to 11 μm) grown in 28 days develops cracks upon drying and can easily detach during storage/manipulation. Ti64(HF-H_2O_2) shows kinetics of hydroxyapatite significantly slower with respect to the other samples, but it is able to develop a hydroxyapatite layer of the same type after 28 days of soaking in SBF.

The chemical stability vs pH was explored by the zeta potential titration measurements and FESEM observation. At this purpose, it is of interest to make a comprehensive discussion of the set of data obtained on the samples as-prepared or soaked for different times: FESEM observation, before and after zeta potential titration measurements. In order to discuss the results of the zeta potential titration measurements, it must be considered that they are performed with a first cycle of washing for the instrument run-up, then the titration of pH starts from pH 5.6, moves towards the basic range (up to pH 9), goes back again at pH 5.6 and finally moves towards the acidic range (down to pH 3), as described in the materials and methods section.

Considering the as-prepared samples, the standard deviation of the zeta potential values is low and constant, no significant variation of the gap between the two samples was registered and no difference was evidenced on the sample morphology before and after the zeta potential titration curves. It can be concluded that the surface and interface between the surface oxide layers and the metal substrate (in the case of the titanium samples) are chemically stable with respect to pH change in the range 3–9.

Differently, the occurrence of some surface reactions and interface instability was detected on the samples soaked in SBF. In the case of Ti64(A-H) and Ti64(A-Ca-H-W), the samples are fully covered by a hydroxyapatite layer after soaking in SBF for 1 (the hydroxyapatite layer is about 2 μm thick) and 7 days (about 3–5 μm), while they result as completely deprived of hydroxyapatite after the zeta potential measurements and they show the morphology of the as-prepared surface oxide layers (FESEM images). Their zeta potential titration curves are significantly different from the as-prepared ones. In the case of the samples soaked for 1 day, no difference in the gap between the specimens is observed during the measurement and this is expected even if some detachment occurs from the surface because of the low thickness of the precipitated hydroxyapatite layer during soaking, but an increment of the standard deviation is observed below pH 4 giving an evidence of a surface reaction. This reaction can be ascribed to the dissolution of the hydroxyapatite layer. In the case of the samples soaked for 7 days, an increase in the gap (up to around 6 μm) between the specimens is observed starting around pH 4 and below this value. All obtained data, can be interpreted considering that the formed hydroxyapatite is dissolved and detached from the substrate when pH goes down below pH 4. The detachment leaves exposed the surface oxide layer with the same morphology of the as-prepared samples, but with a different surface chemistry and an increased number of functional groups (OH) with a strong acidic strength (according to the shift of the IEP towards a lower pH value with respect to the as-prepared samples).

In the case of Ti64(HF-H_2O_2), a progressive shift of the IEP towards higher pH values with respect to the as-prepared sample is observed in the samples after soaking for 1–7 days according to the adsorption of ions and the precipitation of hydroxyapatite crystals during soaking in SBF, even if a continuous layer of hydroxyapatite is not formed. No evident change in the gap between the specimens can be detected on these samples during the zeta potential titration measurements according to the low thickness of the precipitation layers on these samples.

IEP values close to the hydroxyapatite one (around 4.5–4.8) have been observed for Ti64(A-H), Ti64(A-Ca-H-W) and Ti64(HF-H_2O_2) tested after 28 days of soaking in SBF, suggesting that the formed hydroxyapatite layer (observed at FESEM before zeta potential titrations as thick as 11 μm in the case of Ti64(A-H)) is still present on the surface down to that pH (slightly above 4) and, as a consequence, it affects the IEPs and the curve shape in the basic range (presence of a plateau at zeta potential in the range $-16/-33$ mV). The values of standard deviation of the zeta potential suggest that hydroxyapatite has a first limited reaction in the basic range of titration, while at pH below 4 there is a higher rate of reaction and significant dissolution. The relevant increase of the gap between the specimens below pH 4, for Ti64(A-H) and Ti64(A-Ca-H-W) (up to 22 μm) evidences a significant detachment of the surface layers, including both hydroxyapatite and the porous surface oxide layer, as confirmed by FESEM observation after the zeta potential titration measurement (Fig. 8). This effect reveals that, on these samples, the interface between the formed

hydroxyapatite layer and the surface oxide layer is stronger than the interface between the surface oxide layer and the substrate: the detachment of the surface oxide layer occurs when hydroxyapatite is chemically dissolved. In the case of Ti64(HF-H_2O_2), partially dissolution of hydroxyapatite probably occurs, according to the increase in standard deviation below pH 4, but without a significant detachment neither of hydroxyapatite or the surface oxide layer (according to FESEM observation and gap variation between the specimens limited to 6 μm). This effect shows that the mechanism of nucleation of hydroxyapatite, that in this case is related to the presence on the surface of a high density of acidic OH groups completely dissociated at the physiological pH [25], can stabilize the hydroxyapatite layer even if it is of the same type (according to FTIR data) as that developed through different nucleation mechanisms such as ion exchange with SBF.

In the case of Ti(A-HC-H), the obtained data (high standard deviation on almost all points of the titration curves, absence of the hydroxyapatite layer and of most of the porous oxide layer after the zeta potential measurements in the case of all soaked samples, relevant gap variation in the samples soaked for 7 (up to 7 μm) and 28 days (up to 11 μm) at pH 4 and below it, can be explained considering that in this case there is a higher surface reactivity and instability occurring at both the interfaces between the compact and porous oxide layer and the metal substrate or with hydroxyapatite during all the explored pH range. These results are in agreement with the ones previously obtained on analogous samples [51] after in vivo implantation (in physiological conditions, without inflammation). In these conditions, Ti(A-HC-H) surfaces evidenced a fast and strong bone bonding behavior, with the formation of a thicker reaction layer, compared to Ti(A-H) type surfaces. At the meantime, Ti(A-HC-H) surfaces underwent detachment after long time implantation (> 8 weeks) while Ti(A-H) ones did not. These observations evidence that in the case of Ti(A-HC-H) surfaces the bone-reaction layer interface is stronger than the bioactive layer-substrate interface. This phenomenon did not happen on the Ti(A-H) type surfaces, highlighting a stronger bioactive layer-substrate interface.

As far as the BG sample is concerned, the IEP value of all soaked samples is far from the hydroxyapatite one and close to the as-prepared sample, all values of the sample soaked for 1 day have high standard deviation, there is a consistent gap variation between the two specimens (up to 13–15 μm) and high standard deviation below pH 4 on the samples soaked for 7 and 28 days. All these data suggest that also in this case there is a high surface reactivity and instability with hydroxyapatite detachment beginning before the acidic titration and increasing below pH 4 (silica gel layer is still present after the complete titration, FESEM-EDS observations).

It can be concluded that at pH 4, or lower, chemical instability of the precipitated hydroxyapatite can occur and this involves its dissolution in the case of Ti(A-HC-H), Ti64(A-H) and Ti64(A-Ca-H-W) after short times (1–7 days) of soaking in SBF (instability of the material-hydroxyapatite interface). In some cases, detachment of the surface porous oxide layer can also occur with an instability of the material-oxide layer interface: this is the case of Ti(A-HC-H), just at the beginning (1–7 days) of soaking in SBF, or Ti64(A-H) and Ti64(A-Ca-H-W), after long time of soaking in SBF (28 days). Considering that the maturation degree of the hydroxyapatite is almost the same on all surfaces after 28 days (as deduced from the FTIR chemical imaging data), it can be inferred that this parameter does not significantly affect the stability of the hydroxyapatite- bioactive surface layer interface.

Instability of the interfaces of bioactive materials when pH changes in the surrounding fluid occurs without a simple one-to-one dependence from the thickness or mechanical resistance of the surface oxide layer-substrate interface (as obtained from the scratch tests), the presence of different crystalline structure within it or the bioactive mechanism, as it could be speculated before this research work. The highest stability of both the interfaces is observed in Ti64(HF-H_2O_2) which does not register the highest scratch resistance neither at the macro or the micro-scratch test. Ti64(HF-H_2O_2) has a surface oxide layer with submicron thickness, no inner interface between a porous and a compact layer and a single crystalline phase. The bioactive mechanism of Ti64(HF-H_2O_2) is based on electrostatic attraction of ions by the negatively charged surface with a slow kinetics. On the other side, the lowest stability is that of Ti(A-HC-H) which has the lowest resistance to macro scratch test, an oxide layer less thick that Ti64(A-H) or Ti64(A-Ca-H-W) and with a single crystalline phase as well. The bioactive mechanism of Ti(A-HC-H) is based on electrostatic attraction, due to formation of a local microenvironment; it has faster kinetic of hydroxyapatite precipitation than Ti64(HF-H_2O_2), but slower than BG and Ti64(A-H). In conclusion, the presence of a bioactive surface oxide layer thicker than 1 μm with an inner interface can affect the stability of the interfaces of the bioactive material, but it is not trivial to rank the bioactive material in function of stability of its interfaces: a specific protocol of tests is needed at this purpose and similar materials can show different behavior from this standpoint. It is of interest that if we rank the bioactive materials as a function of kinetics of hydroxyapatite precipitation, as the authors made in the previous paper [25], or of interfaces stability, as they do in this research, the rank is significantly different.

Even if the performed tests cannot be considered a true simulation of the physiological condition of a bone implant, these data can be useful in order to evaluate the potential risks of low pH in case of inflammation of a bioactive bone implant.

5. Conclusions

A bioactive glass and four different chemically treated bioactive titanium surfaces have been investigated before and after soaking in SBF (up to 28 days) in order to compare their long term bioactivity, the maturation of hydroxyapatite along time, the mechanical stability of the surface bioactive layer-substrate interface and the chemical/mechanical stability of the grown hydroxyapatite layer (interface between hydroxyapatite and the surface bioactive layer). The combination of several characterization techniques (Raman spectroscopy, macro and micro scratch tests, soaking in SBF, FESEM-EDS, zeta potential electrokinetic measurements and FTIR- chemical imaging) resulted effective for an in depth understanding of the surface stability and reactivity. Macro and micro scratch measurements evidenced differences among the metallic surfaces concerning their sensitivity to localized and distributed surface applied loads which resulted in different scratch resistances in the macro and micro setup. After 28 days of soaking in SBF, all the surfaces, despite of their own kinetics, are covered by a bone like carbonate-hydroxyapatite with B-type substitution. However, the stability of this apatite is not the same for all the materials. A certain dissolution of hydroxyapatite at low pH (around 4, close to inflammation one) has been evidenced for all the tested surfaces, but in a more pronounced way for the ones with faster bioactivity. Moreover, the most reactive surfaces (fast and conspicuous hydroxyapatite precipitation) exhibited also detachment in an acidic environment of the surface bioactive layer together with hydroxyapatite. The obtained results are in agreement with some in vivo results obtained by the same authors and this protocol of characterization can be used in the future to predict the implant-bone interface stability.

CRediT authorship contribution statement

S. Ferraris:Conceptualization, Methodology, Writing - original draft.**S. Yamaguchi**:Conceptualization, Methodology, Writing - original draft, Supervision, Project administration.**N. Barbani**:Investigation, Writing - original draft.**C. Cristallini**:Investigation, Writing - original draft.**G. Gautier di Confiengo**:Investigation, Writing - original draft.**J. Barberi**:Investigation.**M. Cazzola**:Investigation.**M. Miola**:Investigation, Writing - original draft.**E. Vernè**:Writing - original draft, Supervision.**S. Spriano**:Conceptualization, Methodology, Supervision, Writing - original draft, Project administration,

Funding acquisition.

Declaration of competing interest

The authors declare that they have no known competing financial interests or personal relationships that could have appeared to influence the work reported in this paper.

Acknowledgements

This work was supported by MAECI (Ministero degli Affari Esteri e della Cooperazione Internazionale): GLOBAL Project (bilateral projects Italy-Japan; Progetti di Grande Rilevanza Nazionale).

References

[1] B. Kasemo, Biological Surface Science, Surf. Sci. 500 (2002) 656–677.
[2] S. Spriano, S. Ferraris, C.L. Bianchi, C. Cassinelli, P. Torricelli, M. Fini, L. Rimondini, R. Giardino, Bioactive Titanium Surfaces, in Titanium Alloys: Preparation, Properties and Applications, Novapublisher, 2010, pp. 269–293.
[3] V. Guarino, M. Iafisco, S. Spriano, Nanostructured Biomaterials for Regenerative Medicine, Elsevier, 2020.
[4] L. Le Guehennec, A. Soueidan, P. Layrolle, Y. Amouriq, Surface treatments of titanium dental implants for rapid osseointegration, Dent. Mater. 2 (3) (2007) 844–854.
[5] F. Ruppa, L. Lianga, J. Geis-Gerstorfera, L. Scheidelera, F. Hüttig, Surface characteristics of dental implants: a review, Dent. Mater. 34 (2018) 40–57.
[6] S. Ferraris, A. Bobbio, M. Miola, S. Spriano, Micro- and nano-textured, hydrophilic and bioactive titanium dental implants, Surf Coat Tech 276 (2015) 374–383.
[7] E. Matykina, R. Arrabal, M. Mohedano, A. Pardo, M.C. Merino, E. Rivero, Stability of plasma electrolytic oxidation coating on titanium in artificial saliva, J. Mater. Sci. Mater. Med. 24 (2013) 37–51.
[8] J. Katic, A. Šaric, I. Despotovic, N. Matijakovic, M. Petkovic, Ž. Petrovic, Bioactive coating on titanium dental implants for improved anticorrosion protection: a combined experimental and theoretical study, Coatings 9 (2019) 612, https://doi.org/10.3390/coatings9100612.
[9] J. Qi, Y. Yang, M. Zhou, Z. Chen, K. Chen, Effect of transition layer on the performance of hydroxyapatite/titanium nitride coating developed on Ti-6Al-4V alloy by magnetron sputtering, Ceram. Int. 45 (2019) 4863–4869.
[10] M. Fernández-Yagüe, R.P. Antoñanzas, J.J. Roa, M. Biggs, F.J. Gil, M. Pegueroles, Enhanced osteoconductivity on electrically charged titanium implants treated by physicochemical surface modifications methods, Nanomedicine 18 (2019) 1–10.
[11] X. Shen, L. Ping, L. Wang, C. Liu, J. Liu, Z. Deng, Improving the stability and bioactivity of micro-arc oxidized calcium phosphate/titania porous coatings by high energy shot peening pretreatment, Ceram. Int. 46 (2020) 2041–2048.
[12] J. Guillem-Marti, N. Cinca, M. Punset, I. García Cano, F.J. Gil, J.M. Guilemany, S. Dosta, Porous titanium-hydroxyapatite composite coating obtained on titanium by cold gas spray with high bond strength for biomedical applications, Colloid Surf B 180 (2019) 245–253.
[13] E. Vernè, S. Ferraris, M. Miola, G. Fucale, G. Maina, P. Robotti, G. Bianchi, G. Martinasso, R.A. Canuto, C. Vitale-Brovarone, Synthesis and characterisation of bioactive and antibacterial glass-ceramic part 2 – plasma spray coatings on metallic substrates, Adv. Appl. Ceram. 107 (2008) 245–253.
[14] S.R. Paital, N.B. Dahotre, Calcium phosphate coatings for bio-implant applications: materials, performance factors, and methodologies, Mat Sci Eng R 66 (2009) 1–70.
[15] E. Saiz, S. Lopez-Esteban, l S. Fujino, T. Oku, K. Suganuma, A. P. Tomsia, Characterization of metal/glass interfaces in bioactive glass coatings on Ti-6Al-4V and co-Cr alloys, in M.A. Meyers, R.O. Ritchie, M. Sarikaya, Nano and Microstructural Design of Advanced Materials, 2003 Elsevier Ltd.
[16] T. Onoki, K. Hosoi, T. Hashida, Y. Tanabe, T. Watanabe, E. Yasuda, M. Yoshimura, Effects of titanium surface modifications on bonding behavior of hydroxyapatite ceramics and titanium by hydrothermal hot-pressing, Mat Sci Eng C 28 (2008) 207–212.
[17] F.S. Utkua, E. Seckin, G. Goller, C. Tamerler, M. Urgen, Electrochemically designed interfaces: hydroxyapatite coatedmacro-mesoporous titania surfaces, Appl. Surf. Sci. 350 (2015) 62–68.
[18] G.E. Stana, A.C. Popa, A.C. Galca, G. Aldica, J.M.F. Ferreira, Strong bonding between sputtered bioglass–ceramic films and Ti-substrate implants induced by atomic inter-diffusion post-deposition heat-treatments, Appl. Surf. Sci. 280 (2013) 530–538.
[19] A. Madhan Kumara, B. Suresh, S. Das, I.B. Obot, A.Y. Adesina, S. Ramakrishna, Promising bio-composites of polypyrrole and chitosan: surfaceprotective and in vitro biocompatibility performance on 316L SS implants, Carbohydr. Polym. 173 (2017) 121–130.
[20] L. Parisi, A. Toffoli, B. Ghezzi, B. Mozzoni, S. Lumetti, G.M. Macaluso, A glance on the role of fibronectin in controlling cell response at biomaterial interface, Jpn Dent Sci Rev 56 (2020) 50–55.
[21] J.H. Lee, H.-S. Ryu, D.-S. Lee, K.S. Hong, B.-S. Chang, C.-K. Lee, Biomechanical and histomorphometric study on the bone–screw interface of bioactive ceramic-coated titanium screws, Biomaterials 26 (2005) 3249–3257.
[22] J. Chang, X. Zhang, K. Dai, Material characteristics, surface/interface, and biological effects on the osteogenesis of bioactive materials, Bioactive Materials for Bone Regeneration, Elsevier Ltd, 2020, , https://doi.org/10.1016/B978-0-12-813503-7.00001-7.
[23] A. Goharian, Osseoconductivity effects in enhancement of Osseointegration, Osseointegration of Orthopaedic Implants, Elsevier Inc, 2019, , https://doi.org/10.1016/B978-0-12-813384-2.00005-9.
[24] J.E. Samorezov, E. Alsberg, Spatial regulation of controlled bioactive factor delivery for bone tissue engineering, Adv. Drug Deliv. Rev. 84 (2015) 45–67.
[25] S. Ferraris, S. Yamaguchi, N. Barbani, M. Cazzola, C. Cristallini, M. Miola, E. Vernè, S. Spriano, Bioactive materials: in vitro investigation of different mechanisms of hydroxyapatite precipitation, Acta Biomater. 102 (2020) 46 8–4 80.
[26] M. Miola, G. Fucale, G. Maina, E. Verné, Antibacterial and bioactive composite bone cements containing surface silver-doped glass particles, Biomed. Mater. 10 (2015) 055014.
[27] S. Ferraris, S. Spriano, G. Pan, A. Venturello, C.L. Bianchi, R. Chiesa, M.G. Faga, G. Maina, E. Vernè, Surface modification of Ti-6Al-4V alloy for biomineralization and specific biological response: part I, inorganic modification, J. Mater. Sci. Mater. Med. 22 (2011) 533–545.
[28] D.K. Pattanayak, S. Yamaguchi, T. Matsushita, T. Kokubo, Effect of heat treatments on apatite-forming ability of NaOH- and HCl-treated titanium metal, J. Mater. Sci. Mater. Med. 22 (2011) 273–278.
[29] S. Yamaguchi, K. Akeda, K. Murata, N. Takegami, M. Goto, A. Sudo, T. Matsushita, T. Kokubo, Chemical and heat treatments for inducing bone-bonding ability of Ti-6Al-4V pedicle screw, Key Eng. Mater. 631 (2015) 225–230.
[30] European Standard, Advanced Technical Ceramics — Methods of Tests for Ceramic Coatings. Part 3. Determination of Adhesion and Other Mechanical Failure Modes by Scratch Test, prEN1071–3, (1999) (42 pp).
[31] T. Kokubo, H. Takadama, How useful is SBF in predicting in vivo bone bioactivity? Biomater 27 (2006) 2907–2915.
[32] ISO 23317, Implants for Surgery – in Vitro Evaluation for Apatite-Forming Ability of Implant Materials, International Organization for Standardization, Switzerland, 2007.
[33] T. Luxbacher, The ZETA Guide Principles of the Streaming Potential Technique, Anton Paar, Graz, 2014.
[34] S. Ferraris, M. Cazzola, V. Peretti, B. Stella, S. Spriano, Zeta potential measurements on solid surfaces for in vitro biomaterials testing: surface charge, reactivity upon contact with fluids and protein absorption, Front. Bioeng. Biotechnol. 6 (2018) 60.
[35] S. Yamaguchi, H. Takadama, T. Matsushita, T. Nakamura, T. Kokubo, Cross-sectional analysis of the surface ceramic layer developed on Ti metal by NaOH-heat treatment and soaking in SBF, J Ceram Soc Japan 117 (2009) 1126–1130.
[36] D. Bellucci, G. Bolelli, V. Cannillo, A. Cattini, A. Sola, In situ Raman spectroscopy investigation of bioactive glass reactivity: simulated body fluid solution vs TRIS-buffered solution, Mater. Charact. 62 (2011) 1021–1028.
[37] C.M. Botelho, M.A. Lopes, I.R. Gibson, S.M. Best, J.D. Santos, Structural analysis of Si-substituted hydroxyapatite: zeta potential and X-ray photoelectron spectroscopy, J. Mater. Sci. Mater. Med. 13 (2002) 1123–1127.
[38] A. Stoch, W. Jastrzebski, A. Brozek, B. Trybalska, M. Cichocinska, E. Szarawara, FTIR monitoring of the growth of the carbonate containing apatite layers from simulated and natural body fluids, J. Mol. Struct. 511–512 (1999) 287–294.
[39] M. Mujahida, S. Sarfraz, S. Amin, On the formation of hydroxyapatite nano crystals prepared using cationic surfactant, Mater. Res. 18 (3) (2015) 468–472.
[40] K.C. Blakeslee, R.A. Condrate, Vibrational spectra of hydrothermally prepared hydroxyapatites, J. Am. Ceram. Soc. 54 (11) (1971) 559–563, https://doi.org/10.1111/j.1151-2916.1971.tb12207.x.
[41] A. Grunenwald, C. Keyser, A.-M. Sautereau, E. Crubézy, B. Ludes, C. Drouet, Revisiting carbonate quantification in apatite (bio)minerals: a validated FTIR methodology, J. Arch. Sci. 49 (2014) 134–141.
[42] H. Kawahara, D. Kawahara, M. Hayakawa, Y. Tamai, T. Kuremoto, S. Matsuda, Osseointegration under immediate loading: biomechanical stress–strain and bone formation–Resorption, Implant. Dent. 12 (2003) 61–68.
[43] I.A. Silver, R.J. Murrills, J. Etherington, Microelectrode studies on the acid microenvironment beneath adherent macrophages and osteoclasts, Exp. Cell Res. 175 (1988) 266–276.
[44] F. Baino, S. Hamzehlou, S. Kargozar, Bioactive glasses: where are we and where are we going? J. Funct. Biomater. 9 (2018) 25.
[45] A.L. Maçon, T.B. Kim, E.M. Valliant, K. Goetschius, R.K. Brow, D.E. Day, A. Hoppe, A.R. Boccaccini, I.Y. Kim, C. Ohtsuki, T. Kokubo, A. Osaka, M. Vallet-Regí, D. Arcos, L. Fraile, A.J. Salinas, A.V. Teixeira, Y. Vueva, R.M. Almeida, M. Miola, C. Vitale-Brovarone, E. Verné, W. Höland, J.R. Jones, A unified in vitro evaluation for apatite-forming ability of bioactive glasses and their variants, J. Mater. Sci. Mater Med. 26 (2015) 115–125.
[46] H.-M. Kim, H. Takadama, F. Miyaji, T. Kokubo, S. Nishiguchi, T. Nakamura, Formation of bioactive functionally graded structure on Ti-6Al-4V alloy by chemical surface treatment, J Mater Sci Mater Med 11 (2000) 555–559.
[47] D.K. Pattanayak, S. Yamaguchi, T. Matsushita, T. Kokubo, Nanostructured positively charged bioactive TiO2 layer formed on Ti metal by NaOH, acid and heat treatments, J. Mater. Sci. Mater. Med. 22 (2011) 1803–1812.
[48] M. Barletta, V. Tagliaferri, A. Gisario, S. Venettacci, Progressive and constant load scratch testing of single-and multi-layered composite coatings, Tribol. Int. 64 (2013) 39–52.
[49] A. Sroka-Bartnicka, L. Borkowski, G. Ginalska, A. Ślósarczyk, S.G. Kazarian, Structural transformation of synthetic hydroxyapatite under simulated in vivo conditions studied with ATR-FTIR spectroscopic imaging, Article in, Spectrochim. Acta A 15 (2017) 155–161.
[50] H. Madupalli, B. Pavan, M.M.J. Tecklenburg, Carbonate substitution in the mineral component of bone: discriminating the structural changes, simultaneously imposed by carbonate in a and B sites of apatite, J. Solid State Chem. 255 (2017) 27–35.
[51] S. Fujibayashi, T. Nakamura, S. Nishiguchi, J. Tamura, M. Uchida, H.-M. Kim, T. Kokubo, Bioactive titanium: effect of sodium removal on the bone-bonding ability of bioactive titanium prepared by alkali and heat treatment, J. Biomed. Mater. Res. 56 (2001) 562–570.